Fragment Response of Unreinforced Concrete Masonry Walls Subjected to Blast Loading Conditions

by

John Edward Hatfield

A thesis submitted to the graduate faculty of
Auburn University
In partial fulfillment of the
Requirements for the Degree of
Masters of Science

Auburn, Alabama
May 2, 2020

Keywords: Concrete Masonry Unit, Fragmentation, Blast, Fast-Running, Energy Method

Approved by

James S. Davidson, Committee Chair, Gottlieb Professor of Civil Engineering
Robert W. Barnes, Associate Professor of Civil Engineering
Justin D. Marshall, Associate Professor of Civil Engineering
Catherine S. Stephens, Research Civil Engineer Engineering Research and Development Center

Abstract

There are very few methods for predicting the fragment velocity and fragment production of an unreinforced, ungrouted concrete masonry wall. Those that do exist often require large computational resources or fail to predict fragment velocity accurately. A methodology has been developed that accurately and quickly predict the fragment velocity and fragment production of an unreinforced, ungrouted concrete masonry wall. This is an engineering-level analysis tool that can be rapidly implemented and understood. The theoretical background and need for a methodology of this type is discussed. The prediction methodology is compared against two full-scale fragmentation tests conducted in 2019 and four older quarter-scale tests. Reasonable agreement was found between the test results and the energy methodology predictions. As this methodology was developed, it became evident that the negative-pressure time history had a significant impact on the fragmentation behavior. Different methodologies for predicting the negative phase pressure time history were examined and compared. Ultimately no suitable method for predicting the negative phase pressure time history was obtained. The negative phase prediction methodologies and their shortcomings are also discussed and briefly examined.

Table of Contents

List of Tables

List of Figures

List of Abbreviations and Units

Abbreviation	Definition
Avg	Average
CMU	Concrete Masonry Unit
ERDC	U.S Army Engineer Research and Development Center
FEM	Finite Element Method
Pre	Predicted
SDOF	Single Degree of Freedom
TMS	The Masonry Society
TSWG	Technical Support Working Group
URN	Unreinforced and Ungrouted
WAC	Wall Analysis Code
USACE	U.S. Army Corps of Engineers
UFC	Unified Facilities Criteria
Vel	Velocity
t_w	Wall Thickness

Unit Abbreviation	Definition
lb	Pound Force
in	Inch
ft	Foot
ms	Millisecond
sec	Second
psi	Pounds per Square Inch
pcf	Pounds per Cubic Foot

Chapter 1: Introduction

1.1 Background

According to the National Research Council between the year 1982 and 1992 77.5% of all terrorist attacks in the United States were bombings of some type (National Research Council 1995). Blast loading scenarios on civilian structures are commonly the result of terrorist attacks unless a structure is located near an industrial facility with a risk of accidental explosion. According to the National Research Council (NRC), terrorist threats to civilian buildings will continue to be significant because access to commercial buildings is easy. Easy access is a core requirement for many commercial buildings; restricted access would hamper their overall effectiveness as public or commercial spaces. By their very nature, these structures are open to high levels of pedestrian and vehicular traffic. This high trafficability makes the delivery of an explosive device easier and increases the damage potential of a single attack (National Research Council 1995).

The United States Department of Defense has restricted URN CMU from being used in any new construction (Dinan, Fisher, Hammons, and Porter 2003). As stated by Davidson et al. (2005) most injury to the majority of building occupants during an explosive event is not caused directly by the explosive. A great portion of casualties and injuries are caused by the breakup of structural and non-structural elements of the building (Davidson et al. 2005). As building elements, walls, doors, windows, and other loose objects are loaded, they breakup into secondary

fragments. These secondary fragments can cause significant injuries to building occupants and bystanders, since they can be propelled at high speeds by the blast event. Correctly designing building components to withstand extreme loadings without producing deadly secondary fragments is critical for mitigating the casualties and loss of life produced by terrorist attacks or any unintentional explosive events. Similarly, understanding what causes the production of secondary fragments and how they are configured is key to safely mitigating the casualties they can inflict. An understanding of secondary fragment generation is critical to building design, retrofit, and material selection.

The breakup of a structural or non-structural wall constructed of concrete masonry units (CMUs) is a complicated problem; however, it is important to understand the parameters governing this breakup, because the potential damage is great. The increased hazard posed by CMU walls comes from two main factors; they are one of the most common construction materials utilized for wall construction, and they pose an increased fragmentation hazard when compared to similar walls constructed of reinforced concrete. The latter is due to their brittle nature. It is imperative that some method for predicting the level of hazard to building occupants be developed. This will allow for occupants of CMU structures to effectively prepare for blast events and understand the level of potential harm that could be caused. One of the key parameters that influences CMU wall lethality is the fragment field produced by the dynamic breakup of the wall.

1.2 Research Objectives

The objective of this effort was to develop a fast running engineering algorithm to determine if a given concrete masonry wall would produce fragments due to blast loading and to predict the velocity of wall fragments.

1.3 Scope and Methodology

The methodology developed in this work only applies to an unreinforced, ungrouted, non-arching, and one-way acting concrete masonry wall. Specifically, the flexural response until failure and the post failure velocity and distribution of the wall fragments were sought. Wall fragment velocity data is critical for quantifying the hazard posed by a wall explosively loaded until catastrophic failure. Additionally, the goal of this effort was to produce a method of calculation that could generate accurate results quickly without utilizing finite element methods or any intensive computational means of calculation. An analytical tool was produced that can be used on any personal computer. This computational constraint automatically excluded Finite Element Method (FEM) codes like LS-DYNA or the use of a neural network for direct response calculation. Ultimately, an energy balance methodology was utilized that helped overcome the computational constraints while also providing accurate predictions.

To capture the response of the CMU wall before failure, a simple and accurate resistance definition was required. Additionally, the mass and velocities of secondary wall fragments removed from the wall due to blast loading were characterized. Many different responses have been observed during explosive testing of CMU walls. These different wall responses were identified and defined. Finally, the model was validated using fragment velocity data generated from multiple full-scale and quarter-scale experiments.

During the development of the analytical methodology, it became apparent that the fragment velocity was dependent on the negative phase pressure. Methods for predicting the negative phase pressure-time history were explored, but no suitable methodology was obtained. All the methods examined failed to accurately predict the negative phase pressure-time history.

Chapter 2: Literature Review

2.1 Concrete Masonry Research Related to Building a Blast Fragmentation Model

Many efforts have been made to understand the breakup of concrete masonry walls subjected to blast loading (Bewick(a) et al. 2017; Jones 1989). CMU construction is one of the most common construction materials on the planet. CMU walls can be left unreinforced and ungrouted (URN) or grouted and reinforced to varying degrees. Generally, as reinforcing increases, the overall strength and resistance of a CMU wall increases. URN CMU walls are one of the easiest and least expensive wall construction types to produce, but they have virtually no resistance to blast loading. The weakness of URN CMU walls produces two hazards: the breakup of the concrete masonry units into secondary fragments and the removal of a protective structure between building occupants and a threat. The secondary fragments can be quite large and travel at a high velocity, which can pose a serious risk to building occupants.

URN CMU wall types have been utilized in many construction applications that require a level of blast resistance that simple URN CMU walls cannot provide (Davidson et al. 2005); however, it would be prohibitively expensive to demolish and replace all unreinforced walls that require increased blast strengthening. Much effort has been invested in retrofitting techniques for CMU walls that increase their strength and reduce their overall lethality as fragment sources. The largest hazard posed by URN CMU walls is the hazard created by the fragments produced during dynamic breakup. Retrofitting aims to reduce this hazard without completely rebuilding the original wall. As a result, many of the past efforts to understand the behavior of CMU walls

subjected to blast loading aimed to produce an effective retrofit design (Baylot, Bullock, Slawson, and Woodson 2005; Gagnet 2013; Johnson et al. 2009). Predominately, these efforts sought to analyze wall behavior in general or understand wall behavior with a particular type of retrofit installed. The latter was usually to evaluate the effectiveness of a given retrofit material. Most of these efforts utilized finite element methods for analysis and prediction (Davidson et al. 2005; Dennis, Baylot, and Woodson 2002; Eamon, Baylot, and O'Daniel 2004; Magallanes et al. 2008). The response of CMU walls is already quite complex, adding a retrofitting material only serves to increase the complexity of the analysis. As a result, much effort has been expended to analyze the behavior of a CMU wall with a retrofit installed. Very little research has been conducted on the failure and breakup of a non-retrofitted URN CMU walls. Many resistance functions were developed for CMU walls (Department of Defense 2008; Moradi 2007; U.S. Army Core of Engineers Protective Design Center 2008; Wiehle and Bockholt 1968). The work by Gagnet (2013) has an extensive examination and analysis of three resistance functions, but most recent research has focused on modeling CMU walls with retrofitting in mind. No definitive effective model for the failure and subsequent breakup of an un-retrofitted CMU wall has been presented, although some effective partial models do exist. Created by Jones (1989) the Wall Analysis Code (WAC) is the closest complete URN CMU wall failure formulation that was available. However, WAC does not give any indication of how URN CMU walls behave post failure or what level of danger secondary wall fragments might pose. It should be noted that the current version of WAC used by the U.S. Army Corps Engineer Research and Development Center (ERDC) has been heavily modified and provides the user with wall velocities post failure; however, these wall velocity predictions do not match available test data. The thesis that supports

WAC written by Jones in 1989 does not cover any fragment or wall velocity calculations (Jones 1989).

The WAC was created in 1989 by Ann Jones. This FORTRAN code utilized a single degree of freedom methodology to analyze concrete and concrete masonry walls loaded by uniform dynamic air blast. WAC itself was based on programs created by the Stanford Research Institute. Resistance functions were selected for multiple different wall types and support condition configurations. Arching resistance functions were also included in the methodology. The resistance function proposed by Wiehle and Bockholt (1968) was used to analyze simply supported concrete masonry walls. The program also creates a loading function from charge weight and standoff data given by the user. Custom loading functions and resistance functions can also be entered by the user. The current work aims to indirectly expand some aspects of WAC and limit other aspects. The aim of the current effort is to be able to predict the entire response of a concrete masonry wall from the initiation of loading to wall failure and post wall failure. However, the current effort will not encompass as many wall materials or wall support configurations as WAC. The current work is completely independent of WAC, however both works strive to solve similar problems in similar manners. Ultimately, very few efforts have been made to describe the complete failure of a concrete masonry wall outside of a finite element methodology.

No acceptable finite element analysis efforts that attempted to capture the fragmentation response of a CMU wall were found. The work done by Clayton (2008) presented two different methods for calculating fragment masses and velocities of a brittle material. However, this methodology was used to describe a fragmentation event caused by a dynamic impact. The first method was energy based and utilized the information provided by a finite element analysis to

compute a local energy balance and determine fragment mass and velocity. The second method was statistical in nature and relied on the "maximization of a global statistical entropy function"(Clayton 2008) to determine fragment masses and velocities. Ultimately, the goal of avoiding finite element methods for direct computation made both methods unsuitable for use in the current effort. There is very little known about the dynamic breakup of a URN concrete masonry wall.

Some recent attempts have been made to describe the fragmentation response of CMU walls. Bewick(a) et al. (2017); Bewick(b) et al. (2017); Bewick(c) et al. (2018) attempted to encompass the mass and velocity distribution of CMU wall fragments due to blast failure with shock tube testing. The aim of this group of studies was to characterize the breakup of many common construction materials. Multiple small panels of concrete masonry material were loaded until failure by a small diameter shock tube. One full-scale wall was also tested by a large diameter shock tube. Fragment data was collected from both experiments. Mass distribution data was generated by physical collection of fragments. Velocity data was not reliably attained for CMU breakup due to debris obstruction of the high-speed video. Large volumes of dust emanating from the mortar joints can be seen in Figure 1, which likely obstructed the video recording of fragments and resulted in unreliable fragment velocity data.

Figure 1: Initial Breakup of CMU wall with Large Volumes of Dust (Bewick(b) et al. 2017)

The fragment response effort conducted by Bewick(a) et al. (2017); Bewick(b) et al. (2017); Bewick(c) et al. (2018) failed to produce a complete description of dynamic CMU wall breakup. Physical testing limitations resulted in limited velocity data and arduous mass data collection. This exemplifies how difficult experimental data collection of blast induced CMU wall failure can be. The complexity of the wall failure mechanisms combined with the difficulty in collecting data on wall fracture during breakup combine to make understanding the breakup of CMU walls extremely difficult. Figure 2 shows velocity histograms from two separate tests conducted by Bewick(b) et al. (2017) where the midrange velocity fragments were obstructed

from the high-speed camera by dust and a fireball from the shock tube. These velocity measurements were taken from the small-scale shock tube "punch out" tests where a small plate of concrete masonry material was loaded by a small diameter shock tube. The gaps in the center portions of the plots illustrate fragments that were not recorded due to obstruction from dust and fire.

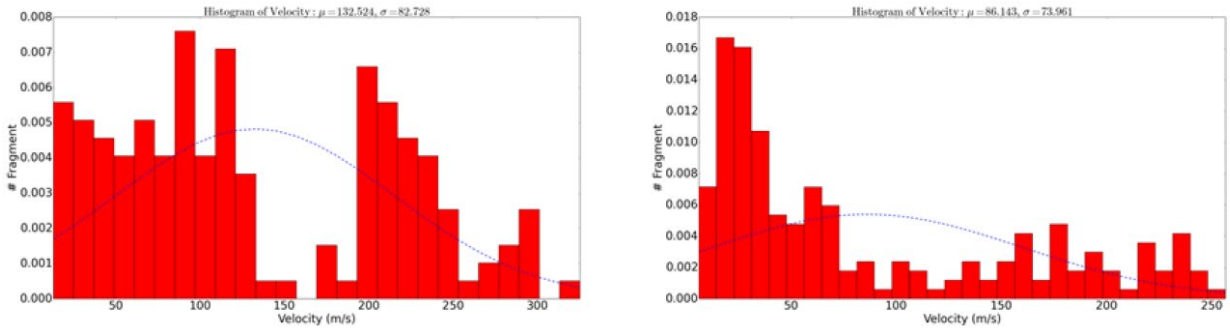

Figure 2: Bewick Velocity Histograms Showing Missing Midrange Velocity from High-speed Video Obstruction from Dust and Fireball (Bewick(a) et al. 2017)

2.2 Dynamic Fragmentation Research

Fragmentation and fracture mechanics have been extensively studied. Many of these efforts sought to explore the nature of fragmentation in a nuclear blast loading environment or due to the breakup of munition casings. These efforts have been ongoing since the advent of nuclear weapons. Several formulations of dynamic fragmentation are energy based Clayton (2008); Englman, Rivier, and Jaeger (1988); Glenn(a) and Chudnovsky (1986); Glenn(b), Gommerstadt, and Chudnovsky (1986); Gommerstadt and Chudnovsky (2005); D. E; Grady (1982, 1988, 1990); Grady(b) and Kipp (1985); Smalley and Woosley (1999); all present energy based formulations of dynamic fragmentation; however, some of the earliest formulations relied on more geometric methods (Grady(a) and Kipp 1985). The energy-based models for dynamic

fragmentation rely on entropy minimization and total energy balance to describe the breakup of a body subjected to highly dynamic loading. Many of these efforts attempted to derive a formula for the average fragment size given the various parameters of the fragmentation event and material being fragmented (Clayton 2008; Englman et al. 1988; Glenn(a) and Chudnovsky 1986; Glenn(b) et al. 1986; Gommerstadt and Chudnovsky 2005; D. E; Grady 1982, 1988, 1990; Grady(b) and Kipp 1985; Smalley and Woosley 1999). One effort even attempted to modify the original Grady methodology to calculate the average velocity of the fragments (Zhang, Lu, and Hao 2004). The drive of these efforts was generally munitions fragmentation characterization; however, some civilian applications were driven by the mining industry (D.E. Grady and Kipp 1980). None of these methods could be directly applied to the breakup of a CMU wall. Many of the fracture phenomenon that affect energy absorption on the small scale are simply not present in the large-scale breakup of a CMU wall. Also, many of the assumptions and formulations made by Grady and his colleagues could not be applied to the macroscale breakup of a CMU wall. However, the current effort asserts that the **general** energy balance formulation presented by Grady and others can be applied to the breakup of CMU walls. This effort seeks to draw inspiration from the energy balance of Grady and others without utilizing their direct means of fragment description.

The work done by Griffith (1921) was foundational to the dynamic work done by Grady. Griffith's crack theory utilized an energy computation to determine if new fracture surfaces would be generated in a material due to applied stress. The theory was first devised due to part failure from cyclical loading. The energy terms and formulations pioneered by Griffith were utilized by Grady for the exploration of dynamic fragmentation problems.

Energy methods for describing dynamic fragmentation had been presented before, but (D. E; Grady 1982) was the first to put terms and direct formulation into a usable and predictive form. Grady's method predicted the average fragment surface area produced by a fragmentation event by balancing the local kinetic energy and surface energy. This method was further improved and solidified by Grady(b) and Kipp (1985) through comparison with limited testing data. Glenn(a) and Chudnovsky (1986) later improved upon Grady's original formulation by adding a stored elastic strain energy term. The Griffith and Grady methodologies were combined by Glenn(b) et al. (1986) into one single formulation. Finally, Englman et al. (1988) presented a single equation to balance the energy of a single fragment. This formulation was solved to yield the average fragment size produced. Similarly, Smalley and Woosley (1999) applied the Grady methodology presented by Englman et al. (1988) to an impactor problem; this illustrates the overall flexibility of an energy formulation. Smalley and Woosley (1999) were able to take the methodology developed by Grady for fragmentation of munitions and apply it to a related but different dynamic fragmentation scenario. The methods surrounding the process of dynamic fragmentation are quite mature.

The overall methodology pioneered by Griffith, presented by Grady, and improved by Smalley, Engleman, and Glenn has potential to hold for the breakup of CMU walls. This methodology serves as the inspiration for the current effort to encapsulate the breakup of a CMU wall. The assumption is that the failure and subsequent breakup of a CMU wall can be described utilizing energy formulations (specifically an energy balance), and that the energy imparted to the wall by blast loading is distributed into different energy absorption mechanisms that describe the entire wall failure response.

2.3 Negative Phase Prediction

The prediction of positive peak pressure and positive impulse can be computed quite consistently and accurately. Figures for predicting positive and negative blast parameters are presented in the UFC 3-340-02 (Department of Defense 2008). In conjunction with the Friedlander curve fit, the positive blast parameters can produce a substantially accurate pressure-time history curve for the positive phase. For most analyses, the negative phase has been neglected (Rigby, Tyas, Clarke, and Fay 2014). This is generally conservative for rigid or hardened structures, but this assumption can be un-conservative for more flexible systems like laminated glass panels (Dharani and Wei 2004; Krauthammer and Altenberg 2000; Teich and Gebbeken 2010). Recently, multiple efforts have sought to produce an accurate pressure time history for the negative phase (Dharani and Wei 2004; Krauthammer and Altenberg 2000; Rigby et al. 2014; Teich and Gebbeken 2010). These efforts have generally used the negative phase blast parameters from UFC 3-340-02 and proposed a function or methodology to construct a pressure-time curve for the negative phase.

Krauthammer and Altenberg (2000) studied the negative phase pressure effects on glass panels utilizing a linear fit to generate a negative phase pressure-time history. Dharani and Wei (2004), also studying the effect of the negative phase on laminated glass, extended the general positive phase Friedlander method into the negative phase. In a more generalized format, Teich and Gebbeken (2010) examined the negative phase from a single-degree-of-freedom model. They extended the Friedlander methodology like Dharani, but also added an additional modification via a scale factor. Rigby et al. (2014) presented their own unique formulation for the prediction of a pressure time history for the negative phase and conducted a study to evaluate

the impacts of neglecting the negative phase. All four methods were compared against pressure data collected by Rigby et al. (2014).

Chapter 3: Energy Method for Finding Fragment Velocity

Broadly speaking, a global energy balance was utilized to capture the fragment responses of a URN CMU wall. Input energy was supplied by an explosive loading event. This input energy was balanced by any output energy from the system. The output energy was separated into two distinct categories, (1) energy absorption mechanisms inside the wall and (2) the kinetic energy of wall fragments. The energy balance was also used to predict wall failure

During the failure of a CMU wall, or any other explosively loaded wall, a specific amount of energy is imparted to the wall by the airblast shockwave. The effects of an explosion result from a shockwave created by a shock front expanding rapidly out from the surface of a given explosive into the surrounding environment (Department of Defense 2008). The loading on the structure results from the reflection of this high-pressure shockwave. This methodology only examines free field airblast and does not include any breaching or ground interaction phenomena. The reflected pressure is a function of explosive type, range, and wall configuration.

The proposed failure theory of a CMU wall is as follows: as the wall is loaded this blast input energy must be dissipated by various energy absorption mechanisms inside the wall system. If there is enough energy absorption potential in the elastic mechanisms, then the wall will simply bend elastically. If all the elastic absorption mechanisms are filled, then the wall will undergo a dynamic fragmentation event. Any energy that has not been used up by the elastic absorption mechanism will be converted into kinetic energy. This kinetic energy causes wall fragments to have significant non-zero velocities. Conversely, if the energy input into the wall

system is not large enough to overcome all the energy absorption mechanisms inside the wall system, then wall fragmentation will not occur.

Dynamic analyses of this type often employ a single degree of freedom (SDOF) analysis methodology. It should be noted that the presented methodology does share some similarities to a SDOF analysis; however, this is not a SDOF analysis tool. At its core, this methodology is simply an energy balance with an adopted resistance function for a concrete masonry wall.

The inspiration for the presented methodology comes from the energy balance, and entropy minimization methods presented by D. E; Grady (1982) and improved by others (Englman et al. 1988; Glenn(b) et al. 1986; Smalley and Woosley 1999). The goal of these works, an effective physical description of the results of a dynamic fragmentation event, is the same as the goal of the current work. However, the specific nature of the breakup of a CMU wall subjected to an airblast is significantly different from the problems these earlier works were seeking to solve.

The breakup of a concrete masonry wall is markedly different from the events described by Clayton (2008); Englman et al. (1988); Glenn(a) and Chudnovsky (1986); Glenn(b) et al. (1986); Gommerstadt and Chudnovsky (2005); D. E; Grady (1982, 1988, 1990); Grady(b) and Kipp (1985); Smalley and Woosley (1999) in several different ways. It should be noted that the following limitations and failure mechanisms are only for an unreinforced, ungrouted, non-arching, one-way, CMU wall. Due to the low strength of the mortar-to-block bond interface, flexural stresses never develop inside the CMUs greater than the elastic limit (Johnson et al.

2009). No flexural stress above the interface strength can be developed in the wall. This stress is significantly lower than the elastic limit stress of the blocks; therefore, no flexural plastic deformations are developed inside the blocks. When CMU walls were dynamically fragmented in testing efforts, the wall fragmented into block size particles. Support for this observation comes from recent tests conducted by the U.S. Army Engineer Research and Development Center (ERDC) in 2019. More details are provided below.

The largest energy absorption mechanism for UNR CMU walls is the elastic strain energy. There is no real plastic strain energy in the wall because no plastic strains are developed in the CMUs; any plastic strains developed in the mortar joints are also assumed to be negligible. By only including the elastic strain energy absorption mechanism in the methodology the velocity of the fragments can be calculated accurately compared to limited test data.

Two testing efforts were utilized to support this investigation. The first and most recent testing effort was conducted by the ERDC in the summer of 2019. Two identical, UNR CMU walls were subjected to two different blast loads. Accelerometers and displacement gauges were used to record wall accelerations and displacements as a function of time. The acceleration data and displacement data was converted into velocity data. Pressure gauges mounted around the perimeter of the wall were used to record pressure data. Additionally, high-speed video of each test was recorded. These tests are referred to as Full-Scale Test 1 and Full-Scale Test 2 both tests were identical in geometry, materials, and setup, except for the loading applied. These tests served as validation for the methodology developed in the effort herein and informed some of the

assumptions proposed. Official reports detailing these tests have not been published at the time of writing, but relevant data will be presented herein. Secondly, multiple tests conducted by the ERDC in 1999 and 2000 for The Technical Support Working Group (TSWG) were utilized for validation. These tests were conducted on quarter-scale UNR CMU walls. The walls were subjected to different far field airblast loadings. Two accelerometers were used to capture the acceleration of the walls, and pressure gauges were arrayed around the perimeter of the wall to record pressure time histories. The acceleration time histories were used to generate velocity time histories for each wall. These walls were also identical in geometry, material properties, and test setup, however their input loadings differed. Many tests were conducted for the TSWG quarter-scale effort; however, only the first four tests are utilized here for validation since they were the only tests in the series that were UNR CMU walls. These tests are referred to herein as Quarter-Scale Test 1, 2, 3, and 4 respectively. Both testing efforts are covered in greater detail below.

3.1 Advantages of Energy Formulation

An energy formulation was utilized in this effort to give an accurate model with reduced computational time. The goal of computational efficiency was not adopted to reduce computational resources for rapid calculation of multiple scenarios, it was adopted to allow the methodology to run effectively on a personal computer within minutes or less.

3.2 Assumptions and Limitations

Specific assumptions about the response of a given CMU wall were required to formulate the presented methodology. These response assumptions were influenced by observations made during the validation testing effort and during the examination of the available historical data. Some assumptions were also necessary for an appropriate energy balance methodology to be formulated with the information available. Appropriate defense for these assumptions is given below. There are limitations in the application and scope to the current effort, which are also defined and explained below.

3.2.1 Assumptions

[1] Each wall fragment is a complete, individual concrete masonry unit.

[2] Energy is distributed uniformly over the wall being analyzed.

[3] Flexural bond strength controls the flexural stress limit.

[4] Flexural stress in blocks never exceeds the elastic limit.

[5] Static flexural strain energy is a good approximation of the amount of dynamic energy absorbed by the wall during loading.

Assumptions about the configuration and behavior of the CMU wall during breakup were required to accurately model the wall's failure. The principal assumption is that during breakup of an ungrouted CMU wall, every fragment is a single CMU and no CMUs are broken by the fragmentation event. The wall breaks along the mortar lines and not through the CMUs. This

assumption came from the observed mechanical behavior of the wall during breakup. When the wall underwent failure, it fractured along the mortar lines and produced fragments that were full blocks. This phenomenon was observed during testing and is also supported by similar observations made by Magallanes et al. (2008). High-speed video from both validation testing efforts were evaluated to reach this conclusion. Additionally, the current state of the art surrounding this phenomenon required an assumption about fragment size since no reliable prediction method existed outside the work done by Bewick(b) et al. (2017). The work done by Bewick was not used because of the testing limitations addressed above and the discrepancies between Bewick's fragment size observations and the observations made during the current validation testing effort. The differences in observations arose from the difference in loading and wall configuration. Bewick's walls were loaded via a shock tube, and they were minimally reinforced. The small-scale experiments conducted by Bewick directly fragmented panels made from concrete masonry unit material with a pressure wave. The CMU material fracture phenomenon was not observed during the validation effort. Instead, the wall fractured along the mortar joints. This assumption only holds for UNR CMU walls. Other wall configurations and loadings may not exhibit this fragmentation behavior.

The main support for the first assumption comes from the high-speed video captured during the two full-scale ERDC tests conducted in the summer of 2019. The test particulars will be discussed later in Chapter 5: Comparison and Validation. Figures 3, 4, and 5 all show different video captures taken from high-speed video recordings. These figures provide evidence

for the assumption that the wall fragments along its mortar lines and the blocks remain unbroken until they impact the floor.

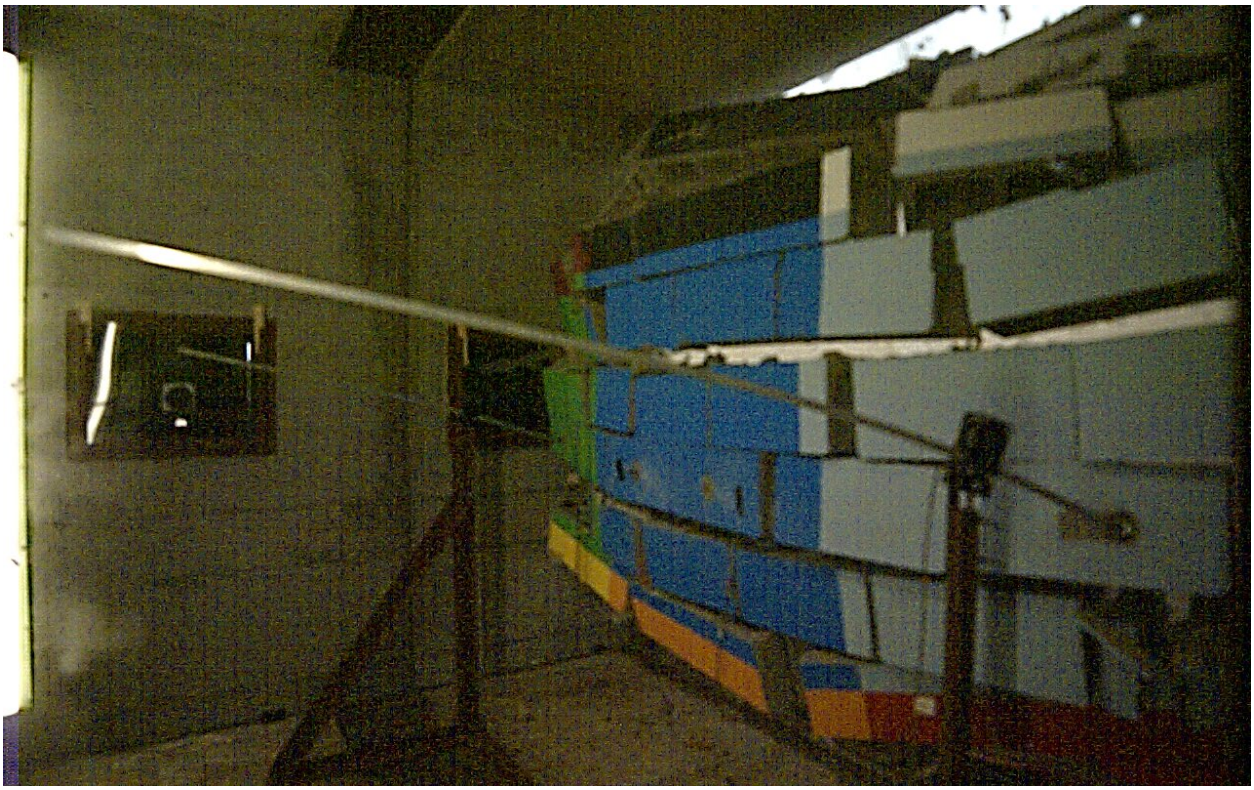

Figure 3: Full-Scale Test 1 Unreinforced CMU Wall Block Separation Side View (ERDC Test 2019)

Figure 4: Full-Scale Test 1 Unreinforced CMU Wall Block Separation Back View Early Time (ERDC Test 2019)

Figure 5: Full-Scale Test 1 Unreinforced CMU Wall Block Separation Back View Late Time (ERDC Test 2019)

This assumption is also supported by work done by Magallanes et al. (2008) Many of the blocks are not broken when the wall undergoes failure and those that are fragmented are in shear failure zones (Magallanes et al. 2008). This describes a test conducted on UNR CMU walls. Figure 6, 7, and 8 are taken from Magallanes et al. (2008) and show the failure of an UNR CMU wall during failure. Careful analysis of the images and Magallanes's report both support the assertion that when an UNR CMU wall undergoes dynamic breakup the fragments are generally block sized. This seems to result from cracks forming along the mortar joint block interface

lines. The wall in Figures 6, 7, and 8 appears to predominantly crack at the 1/3-height and 2/3-height mortar joints, which Magallanes points out. This does not align with the assumed mechanics of the current effort (that the wall predominantly cracks at the mid-height). However, this discrepancy does not discount the support for the current assumption regarding fragment size.

Figure 6: Early Time URN CMU Wall Failure (Magallanes et al. 2008)

Figure 7: Mid Time URN CMU Wall Failure (Magallanes et al. 2008)

Figure 8: Late Time URN CMU Wall Failure (Magallanes et al. 2008)

The energy imparted to the wall from the airblast loading is assumed to be uniformly distributed over the wall. The effects of charge shape such as cylindrical, hemispherical, spherical, or breaching charges were not directly accounted for in this methodology. Similarly, the airblast source was assumed to be far enough away from the wall which minimizes any breaching effects. The loading was modeled as a simple uniform airblast. As a result of the first assumption, each fragment produced is uniform in size (one CMU). When assumption number one is combined with assumption number two each fragment of equal size is imparted with an identical kinetic energy. As a result, a single fragment velocity is predicted for each unit in the entire wall. This ultimately results in a uniform velocity prediction for the entire wall. From this combination, one velocity value is assumed to describe the entire velocity response of every wall

fragment. In reality every wall fragment does not have the same velocity; however, the velocity predictions from this assumption do agree with available testing data so the prediction methodology does give an accurate effective average fragment velocity.

Approximate uniform wall velocity was observed in the supporting experimental results. Multiple discrete measurement points on the validation walls yielded velocity data. The velocity values were generally similar in magnitude 15 to 20 ft/sec of each other. However, the velocity predicted by this methodology only gives one value for the fragment velocity of a wall. It was assumed that this predicted value mirrors the velocity of the midspan of the wall, which appears to be a good indication of the wall velocity in aggregate. Ultimately, this method is approximate in nature and no valid methodology was devised to allow for accurate prediction of multiple fragment velocities. Individual velocity measurement are displayed with the predicted velocities in Chapter 5: Comparison and Validation, to give some idea of the distribution of wall velocities.

The bond strength between mortar and CMUs controls the flexural tension stress that can be carried by the wall (The Masonry Society 2016; Wiehle and Bockholt 1968). The bond strength is significantly weaker than the tensile material strength of either the mortar or the block. Some resistance methodologies even neglect this minimal strength (Moradi 2007). Ultimately, an URN CMU wall is very weak when subjected to out of plane flexure. The blast load can be modeled by an out of plane distributed load when calculating the wall resistance. According to the adopted Wiehle and Bockholt (1968) resistance function the tension resistance is the limiting parameter when calculating wall resistance. The bond strength between the mortar

joint and the block is assumed to be the limiting tension resistance. Selection of this bond strength is discussed in Section 3.3.1 Selection of Tensile Strength (f_r) and Other Material Properties.

The flexural stress inside the wall will not exceed the elastic limit of the blocks. This assertion follows from assumption three, if the stress limit imposed by the bond strength is significantly lower than the elastic stress limit of the block then the blocks will always behave elastically. Since the wall behavior is dominated by block behavior the wall in aggregate is assumed to behave elastically. For the analysis of an URN CMU wall, the elastic stress limit of the blocks is well above the bond strength of the mortar and block. This assumption allows the current methodology to exclude any plastic energy absorption mechanisms.

It was assumed that the static flexural strain energy of a beam in bending was an adequate description of the elastic strain energy present in a CMU wall subjected to blast loading. Many methods of analyzing a CMU wall during an explosive loading event involve the assertion that the wall behaves in a flexural mode, to varying degrees (Jones 1989; Moradi 2007; Wiehle and Bockholt 1968). From this assertion, it seemed reasonable to assume that the strain energy for the wall could be approximated using the flexural beam assumption. Since the wall resistance was being modeled as a beam in flexure, the strain energy was also calculated using this methodology. The secondary resistance strain energy was calculated by assuming both halves of the wall rotated as rigid bodies about their supports. For both resistance mechanisms, the energy absorbed was calculated in a method mechanically consistent with the assumed resistance

function. Different methods were explored for calculating the elastic strain energy of the wall; they are presented later.

3.2.2 Limitations

The methodology developed applies to a limited number of scenarios. The explosive source must be far enough away from the wall being analyzed to result in far field loading. No breaching effects were accounted for. Similarly, no incident angle effects were included in the analysis, so the airblast shock wave is assumed to impact the wall perpendicularly. This methodology should only be applied to walls that cannot undergo arching. The arching phenomenon was not accounted for in the development of this methodology. Typical 8 by 8 by 16 inch full-scale and quarter-scale CMUs were used in the validation testing effort, and this methodology was developed for use with those typical blocks. More testing should be conducted to confirm that this methodology can be applied to other types of CMUs. The wall must be unreinforced, ungrouted, and one-way acting. All calculations are general and can be applied to any CMU wall that meets the limitations and assumptions of the methodology.

3.3 Mechanics

A mechanical framework was required to dictate structural responses. Ultimately, the wall was treated as a simply supported beam with an applied distributed load. Generally, analyzing a wall of this type is done in terms of a unit beam one measurement unit wide (generally one inch or foot). Since a CMU wall is made up of discrete blocks that are generally nominal 16 inches wide and do not have uniform cross sections, the analysis utilized a unit beam

that was one block wide, simply supported, and loaded with a uniform distributed load as shown in Figure 9.

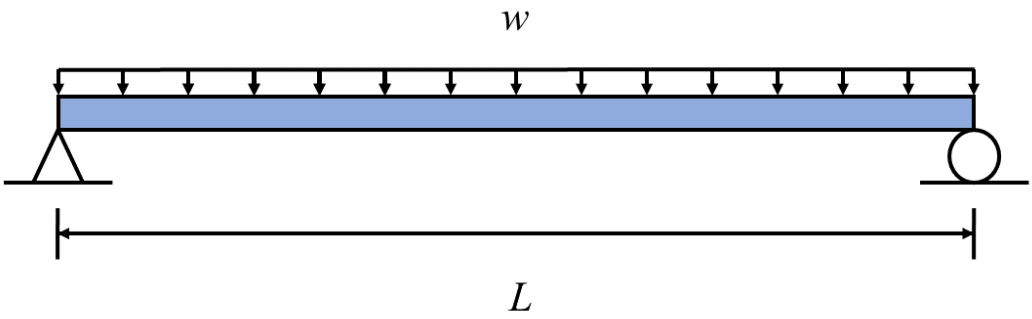

Figure 9: Unit Beam Support Conditions and Loading

The resistance function presented by Wiehle and Bockholt (1968) and adopted for calculating the strain energy in the present study has inbuilt assumptions about the mechanical behavior of the wall. The resistance of the wall is related to the applied load by Equation (3.1)

$$Q_i = w_i L \tag{3.1}$$

where L is the length of the beam (height of the wall) and w is the applied distributed load in force per length units. During the initial elastic resistance phase the wall behaves in a flexural bending mode. The flexural mode ends when the elastic stress limit is reached at the midspan of the wall. At this point the wall is cracked at midspan through its entire thickness and the elastic resistance (Q_1) is at its maximum value. The wall transitions into the secondary resistance phase

after it cracks at midspan. During the secondary resistance phase the wall behaves as two rigid bodies rotating about their supports. The secondary resistance (Q_2) is at its maximum value at the elastic deflection limit. The weight of the wall and the applied vertical force provide a restoring force as the wall deflects. This provides a decaying secondary resistance until the wall deflects one wall thickness. For the validation efforts, all applied vertical loading was assumed to be zero. At some point, the amount of vertical loading applied will likely cause arching. Vertical loadings should be neglected to give the lowest possible flexural resistance. Neglecting vertical loadings should result in higher predicted velocities, which has been deemed preferable. Past one wall thickness the mechanism becomes geometrically unstable, and the wall provides no further resistance. The two behavior models are presented below in Figure 10.

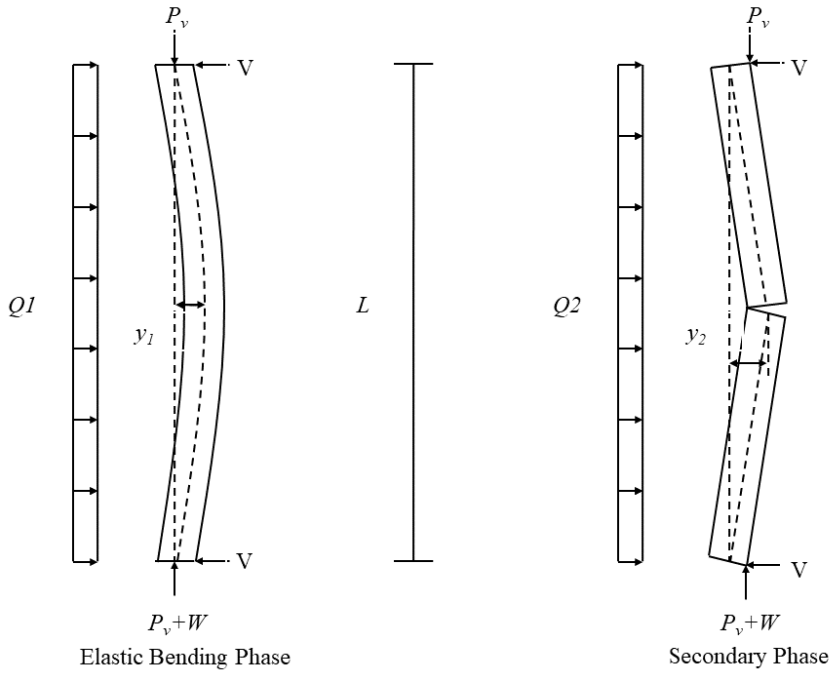

Figure 10: Resistance Models for Elastic and Decaying Phase of Non-arching Wall modified from Wiehle and Bockholt (1968)

The resistance functions derived by Wiehle and Bockholt (1968) are presented below in Equation (3.2) and Equation (3.4) where the elastic resistance is given by Q_1, maximum elastic displacement is given by y_1, self-weight is given by W, shear force is given by V, secondary resistance is given by Q_2, secondary displacement is given by y_2, wall thickness is given by t_w, limiting tensile stress of the wall is given by f_r, and applied vertical load is P_v. The maximum elastic displacement is given by Equation (3.3). The formulations for Q_1 and y_1 can be found quite easily via simple beam mechanics. Any eccentricity in the load P_v, as well as the wall self-weight W is neglected for the calculation of Q_1. Establishing the value for Q_2 is more involved.

$$Q_1 = \frac{16I}{t_w L}\left(f_r + \frac{P_v}{A}\right) \tag{3.2}$$

$$y_1 = \frac{5}{384}\frac{Q_1 L^3}{E_c I} \tag{3.3}$$

$$Q_2 = \frac{4}{L}(t_w - y_2)(W + 2P_v) \tag{3.4}$$

The system must be treated as two independent rigid bodies. By examining the top section and bottom section independently, two separate resistances can be calculated. Summing moments about the bottom support yields Equation (3.5) and summing moments about the top support yields Equation (3.6). The self-weight of the wall is not neglected for the secondary resistance calculation. The weight of the bottom half of the wall provides more secondary resistance when the resistance is split out this way. Adding both the top and bottom resistances together results in the resistance formula shown in Equation (3.4).

$$Q_{bot} = \frac{4}{L}(t_w - y_2)(\tfrac{3}{4}W + P_v) \tag{3.5}$$

$$Q_{top} = \frac{4}{L}(t_w - y_2)(\tfrac{1}{4}W + P_v) \tag{3.6}$$

$$Q_2 = Q_{bot} + Q_{top} \tag{3.7}$$

The elastic resistance and secondary resistance functions will yield a discontinuity at the transition point between the two functions. If the secondary resistance at the transition point is

lower than the elastic resistance, then the resistance value decreases instantaneously from the elastic value to the secondary value. If the secondary resistance is greater than the elastic resistance at the transition point, then the elastic resistance value will continue to increase at the current rate until the elastic resistance equals the secondary resistance at the given wall deflection. For an unreinforced CMU wall, the secondary resistance will always be significantly lower than the elastic resistance unless a significant vertical load is applied. This transition is illustrated in Figure 11.

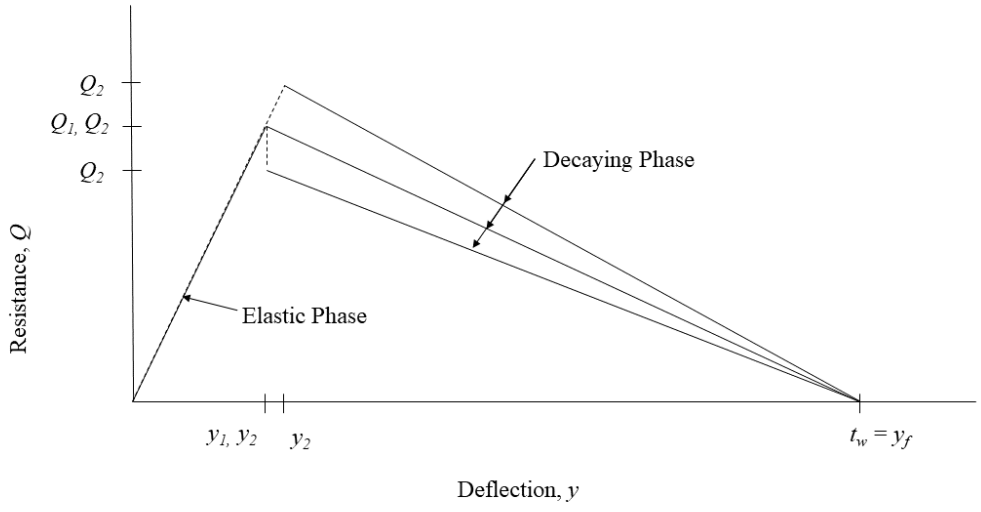

Figure 11: Resistance function transition for one-way, non-arching, URN CMU wall modified from Wiehle and Bockholt (1968)

To avoid confusion and illustrate the difference between the strain energy absorbed by the elastic phase and the secondary resistance phase, a plot of Figure 11 using the full-scale test 1 wall parameters is given in Figure 12. The maximum resistance in the elastic phase is significantly larger than the secondary resistance, but it is active over an extremely small displacement compared to the width of the block. Conversely, the maximum secondary resistance is much lower than the elastic resistance. The secondary resistance is about 6% of the elastic resistance, but it is active over almost the entire deflection of the wall. As a result, the energy absorbed by the secondary phase is significantly larger than that absorbed by the elastic phase.

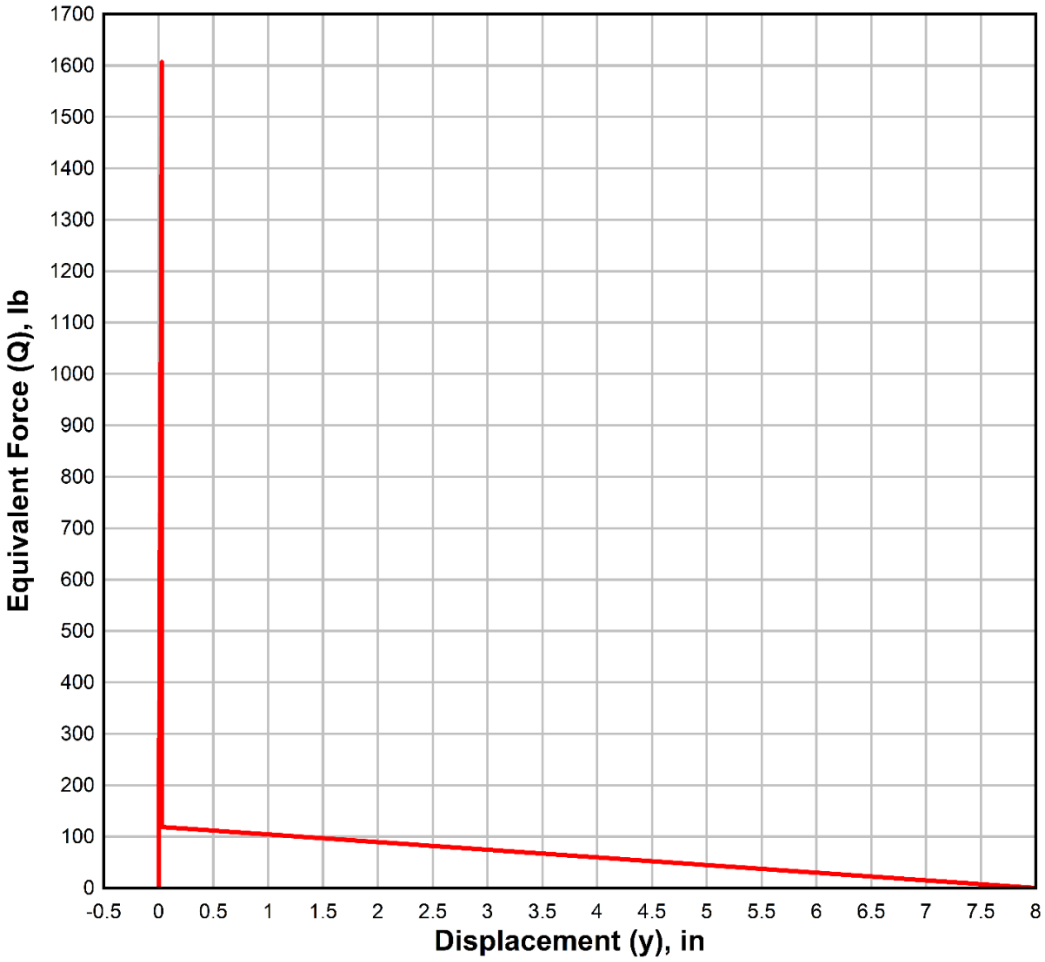

Figure 12: Elastic and Secondary Resistance to Scale for the Full-Scale Test 1 Wall

This effort pulls extensively from the work done by Jones (1989) to formulate the WAC. Jones used the Wiehle and Bockholt (1968) resistance functions for an UNR CMU wall. The secondary resistance function presented by Jones (1989) differs from the one presented in Equation (3.4) by a factor of one half. It is not clear where this difference originates from.

3.3.1 Selection of Tensile Strength (f_r) and Other Material Properties

The selection of a tensile strength limit is required to calculate the maximum elastic resistance of a CMU wall in the Wiehle and Bockholt (1968) method. For an UNR CMU wall, the tensile strength and vertical applied load are the main two parameters that contribute to the strength of the wall during the elastic resistance phase. If no vertical load is applied, then the controlling tensile strength is the only parameter that affects the elastic resistance. Wiehle and Bockholt (1968) states that the modulus of rupture or the tensile bond strength may be used for the tension limit in Equation (3.2). For an UNR CMU wall, the tensile bond strength between the mortar and the blocks will always be lower than the modulus of rupture of the concrete masonry units. Therefore, the bond strength limit was be employed for this effort.

There is some discord regarding the selection of a tensile bond strength limit in the literature. Johnson et al. (2009) uses a "modulus of rupture of mortar" of 65 psi for their analysis. They also use the resistance functions presented by Jones and employed in WAC to capture the resistance of a non-arching, UNR CMU wall. Dennis et al. (2002) utilized the same quarter-scale data that is used for validation in this thesis to validate a finite element methodology. They employed a "tensile strength" of 250 psi (nominal) and 225 psi (reduced). During the analysis Dennis et al. (2002) conducted, they reduced some of the material parameters and conducted a second analysis to try and make their predicted displacement response match the observed response more closely. Dennis et al. (2002) describes the material properties they utilized as: having a large variability in available standards which shows the challenges encountered when

analyzing existing masonry walls. The tensile strength of the CMUs used in the quarter-scale test was not reported so an estimate of their strength was made by Dennis et al. (2002).

The Methodology Manual for the Single-Degree-of-Freedom Blast Effects Design Spreadsheets (SBEDS methodology manual) gives the tensile strength of mortar in running bond between 30 psi and 50 psi (U.S. Army Core of Engineers Protective Design Center 2008, pp. 7-51); however, it suggests that for dynamic brittle analysis of unreinforced CMU walls, a tension strength of 200 psi to 250 psi be used if no other data is available. The UFC 3-340-02 does not mention a tension resistance of unreinforced CMU walls (Department of Defense 2008, p. 1629).

Finally, The Masonry Society 402/602-16 recommends a tension strength value of 84 psi for hollow ungrouted units with type M or S Portland cement/lime or mortar cement type mortar. Similarly, for units with type N Portland cement/lime or mortar cement type mortar a modulus of rupture value of 64 psi is recommended.

For the validation efforts presented below, a tensile strength limit of 200 psi was employed. This value was selected as the limiting stress of a glue like bond between the mortar and block. This bond strength is highly variable because the bond is created by mortar intrusion into the porous block structure (Ahmad 2018). The bond strength is likely different for each individual block in a given wall. The low values reported by the The Masonry Society (2016) are given as design values; they were considered to be overly conservative for the given analysis.

Ultimately, the bond strength has a miniscule effect on the velocity of a wall that is well inside the loading regime for wall fragment production and failure. The bond strength has a more

significant influence on the velocity of walls that are just inside or outside the loading regime for wall fragment production and failure. Additionally, the bond strength parameter affects the amount of input energy required to reach the fail and non-fail point.

3.4 Energy Balance Theory

3.4.1 Introduction

As stated above, many individuals have described the dynamic breakup of a material utilizing energy formulations. D. E; Grady (1982) was one of the first to examine this methodology. Grady's method was finalized by Englman et al. (1988). However, the methods used by Grady and his contemporaries only apply to dynamic fragmentation situations that are markedly different from the breakup of a CMU wall. Their equations could not be directly applied, but the general methodology was adopted for the current effort.

The effort herein assumes that during the failure of a CMU wall, or any other wall loaded by airblast, a specific amount of energy is imparted to the wall by the reflection of the airblast. This imparted energy is a function of explosive type and configuration. As the wall is loaded, this imparted energy must be dissipated by energy absorption mechanisms inside the wall system. If there is enough energy absorption potential in the elastic absorption mechanisms, then the wall will simply bend elastically. If all the elastic mechanisms are expended, then plastic mechanisms may absorb some additional energy. Finally, if both the elastic and plastic energy absorption mechanisms are overwhelmed, then the wall will undergo a fragmentation event, and any energy that has not been used up by an elastic or plastic mechanism will be converted into

kinetic energy. This kinetic energy is what causes wall fragments to have significant non-zero velocities. Since the stress inside the wall is assumed to never exceed the elastic limit, plastic energy absorption mechanisms are neglected.

The energy input into the wall system is balanced against the energy absorbed by the system. The methods presented by Grady and others made similar assertions (Clayton 2008; Glenn(a) and Chudnovsky 1986; Glenn(b) et al. 1986; Gommerstadt and Chudnovsky 2005; D. E; Grady 1982, 1988, 1990; Grady(b) and Kipp 1985; Smalley and Woosley 1999); however, they had significantly more absorption mechanisms. The energy input into the system comes from the reflected pressure of the airblast. For the current methodology, energy is absorbed in three ways. 1) Energy is absorbed by the elastic flexural response of the wall. The strain energy of the wall at tensile bond failure is assumed to be a good approximation of this energy absorption. 2) Energy is absorbed by the rigid body rotation of the top and bottom wall halves. Similarly, the work done by the two rotating bodies is taken to be a good approximation of this energy absorption. This energy absorption mechanism is active from the tensile bond failure to geometric instability which occurs at one wall thickness of deflection which corresponds to zero wall resistance. 3) After wall failure, energy is "absorbed" by the wall fragments and is converted into kinetic energy. This kinetic energy results in wall fragments having non-zero velocities. The energy balance utilized in this effort is presented below in Equation (3.8).

$$E_{in} = E_{ke} + E_{absorbed} \tag{3.8}$$

Where E_{in} is the energy imparted to the system from the blast wave, E_{ke} is the total kinetic energy of the wall, and $E_{absorbed}$ is the energy absorbed by the wall via the different energy absorption mechanisms as it deflects.

3.4.2 Input Energy

The shape of a pressure-time history curve for the given scenario is well defined. The shock front increases the pressure at the wall almost instantaneously. The increasing pressure is due to the airblast from the explosive. The value of the peak pressure is dependent on the charge weight and standoff. The peak pressure quickly decays. Once the pressure value is below the ambient pressure, it is in the negative phase. During this phase, the structure undergoes a pressure that is less than the atmospheric pressure. The negative phase is generally much longer in duration and much smaller in peak magnitude compared to the positive phase. The structure is subjected to a pressure much greater than atmospheric by the positive phase and then experiences a pressure below atmospheric by the negative phase. The general shape of a pressure time history is given below in Figure 13.

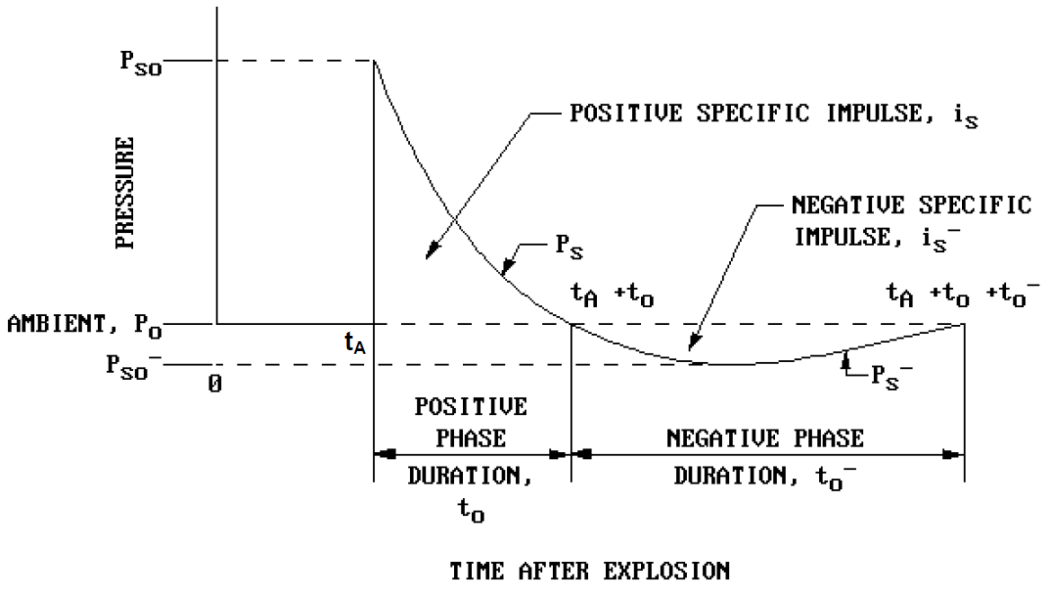

Figure 13: Typical Free-field Pressure Time History (Department of Defense 2008)

For many structures, the negative phase can be neglected for analysis. However, for flexible structures, cladding type structures, and glass it is important to include the negative phase pressure (Dharani and Wei 2004; Krauthammer and Altenberg 2000; Rigby et al. 2014; Teich and Gebbeken 2010). Similarly, it is important to include the negative phase in the current analysis. The negative phase pressure has a pronounced effect on the velocity of the wall. By taking the impulse at the end of the negative phase and using it to calculate the input energy, both the positive and negative phase pressures are accounted for in the input energy. Using only the positive impulse to predict fragment velocity would greatly overpredict the free flight velocity of fragments as supported by observations made during validation testing. During the positive phase, the wall velocity increased rapidly. The negative phase loading decreased the

wall velocity over time. After the end of the negative phase, the wall velocity leveled off and remained relatively constant. Figure 14 shows a typical velocity time history for an unreinforced CMU wall failure. This time history was taken from the full-scale ERDC Test 1. From 0.15 time to about 0.25 time the blast pressure is positive and the wall velocity increases. After 0.25 time to around 0.60 time the negative phase occurs, and the wall velocity is significantly reduced. Finally, after 0.60 time the wall velocity becomes relatively stable. The stable velocity indicates that any fragments that were created during the breakup of the wall are in free flight. Velocity reduction due to drag is not considered in the free flight calculation since the predicted free flight velocity occurs at the end of the negative phase before air resistance effects have become significant compared to the velocity change imparted by the airblast. After the free flight velocity prediction air resistance must be accounted for to give accurate fragment behavior; however this is outside the scope of the current effort. This velocity stabilization corresponds to the end of the negative pressure phase. By predicting the fragment velocity at the end of the negative phase the free flight fragment velocity can be predicted.

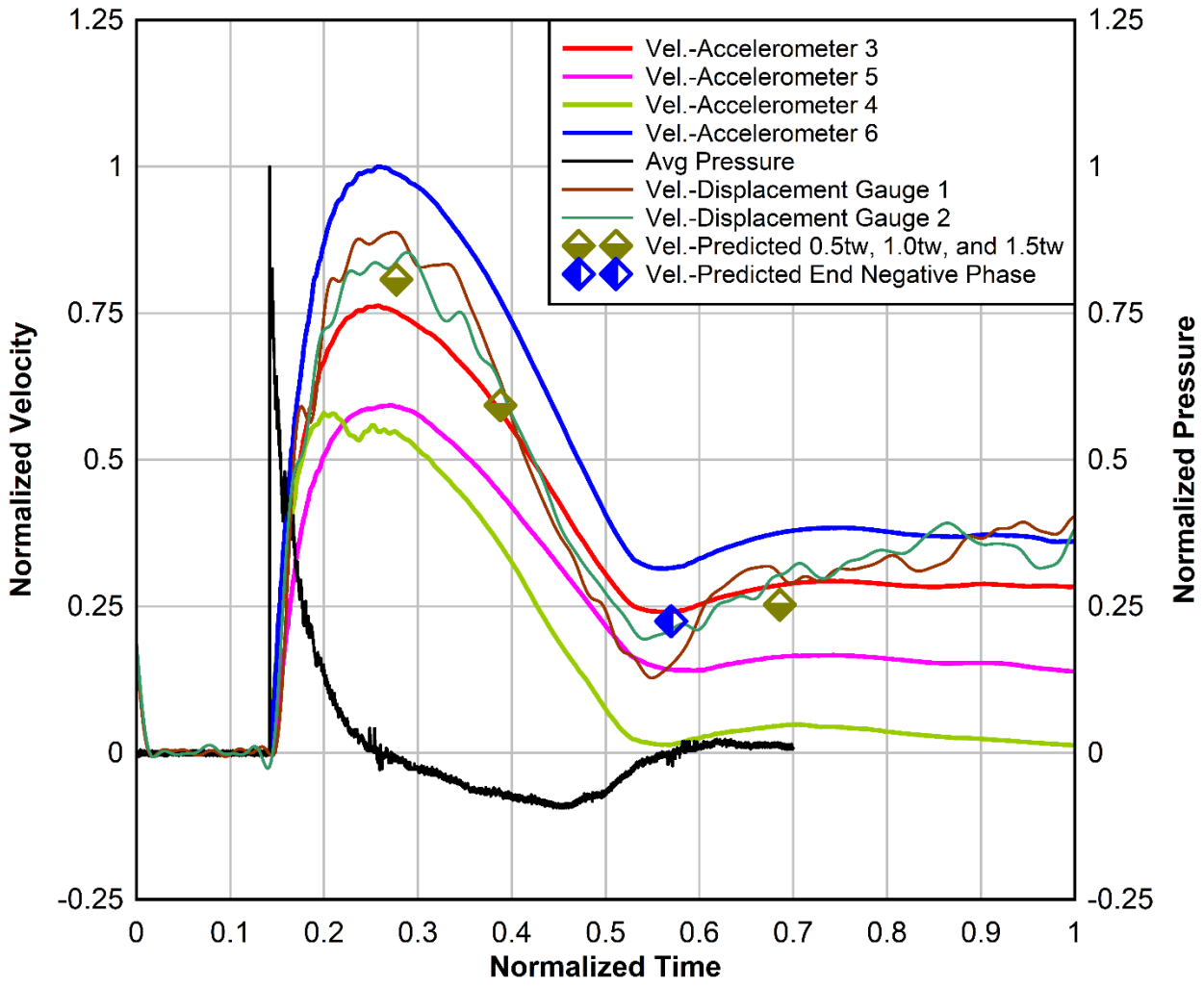

Figure 14: Typical Pressure- and Velocity-Time History for an Explosively Loaded URN CMU Wall

The input energy is given by Equation (3.9) (Biggs 1964, p. 223) where E_{in} is the energy input to the wall by the reflection of airblast pressure, I is the specific impulse of the reflected pressure wave. The impulse has units of [Force-Time]. M is the *total* mass of the wall.

$$E_{in} = \frac{I^2}{2M} \tag{3.9}$$

The Equation (3.9) is presented by Biggs (1964) in order to calculate the kinetic energy of a system with an impulse-dominant load, which is achieved by using a very short duration load. Equation (3.9) is derived by substituting Equation (3.10) into the standard equation for kinetic energy given by Equation (3.11) (Biggs 1964, p. 40)

$$V = \frac{I}{M} \tag{3.10}$$

$$E_{Kinetic} = \tfrac{1}{2} M V^2 \tag{3.11}$$

where V is the velocity of the structure, I is the specific impulse of the blast wave and M is the mass of the wall. Yong (2007) uses a similar method to calculate the fragment velocity of a vented concrete structure and employs a similar energy balance methodology.

The point in time where the energy balance is conducted dictates the time where the velocity is predicted. The total energy balance can be calculated at any time during the system response if there is serviceable impulse data. For each impulse value, a unique velocity can be predicted. Utilizing this fact, a full velocity time history can be constructed for a given wall and loading. If an impulse data value can be obtained, then a corresponding velocity value can be predicted. Once the maximum resistance is achieved, all other required inputs for the energy absorption mechanisms are material or geometrically dependent and do not change with time. According to the adopted resistance function all the energy absorption mechanisms stop

absorbing energy once the wall deflects past roughly one wall thickness, because the wall no longer provides any resistance. As will be shown later, the end of the negative phase generally occurs well after one wall thickness of deflection. During the initial positive pressure phase of loading the wall is imparted with considerable velocity. As the loading continues into the negative pressure phase that velocity is reduced by the negative impulse. After the initial positive pressure loading and negative pressure reduction, the velocity of the wall is roughly constant. At this point, most of the meaningful loading on the wall from the blast event has stopped. If the wall has failed, the fragments (CMUs) are in free flight. The fragment velocity will be further reduced by air resistance until the fragments impact the ground or an obstruction. Utilizing the impulse at the end of the negative phase allows the methodology to encompass both the positive pressure and negative pressure effects of a typical blast event.

It was observed through testing that during the loading of the CMU wall, the blocks on the top and bottom rows were crushed during loading. This behavior was observed during the full-scale ERDC test 1 and 2. This is due to the configuration of the support conditions. Steel angles were used to provide lateral support at the top and bottom of the wall for the two full-scale UNR CMU tests conducted by ERDC. The support conditions restrained the lateral movement of the blocks, which resulted in no horizontal velocity. This phenomenon is captured by removing the top and bottom row of blocks from the energy input calculations. Because the top and bottom blocks do not move, they cannot have any residual kinetic energy so including them in the energy balance would be incorrect. The mass of the wall is reduced by two rows of blocks, and the area which the impulse is applied over is reduced by two rows of blocks also. In

effect, the energy which can contribute to wall failure, and fragmentation is only the energy imparted to the blocks whose lateral movement is not restricted by the support conditions.

It should be noted that the reduction in wall size is not implemented in the resistance functions for calculating the energy absorbed by the wall. The wall height and wall weight utilized in Equations (3.2) and (3.4) are not reduced in any way. The top and bottom rows of CMUs do not move, and they also supply the necessary connection to the wall support conditions. If the top and bottom rows are removed from the flexural calculation, then the wall is effectively unsupported and becomes unstable. This contradicts the assertion of the adopted resistance formulation, which requires pinned support conditions for both the primary elastic response and the secondary rigid body response. The ability of the top and bottom blocks to provide connection to the support conditions is unrelated to their ability to become fragments with non-zero velocities. The assumed boundary conditions are integral to the operation of the adopted resistance functions.

There are many different connection configurations available for concrete masonry construction. Particular attention should be paid to wall construction and detailing so that the effects of wall supports are correctly accounted for. Most wall configurations that can be modeled as simple supports will likely impede the motion of the top and bottom row of CMUs to some degree. However, this may not always be accurate. Each case should be evaluated individually, and the wall area and mass should be reduced accordingly.

Figures 15, 16, and 17 show typically used connection details for CMU construction (National Concrete Masonry Association 2003). In each of these different scenarios some portion of the supporting concrete masonry units will be impeded by the surrounding supporting material. Floor slabs, supporting beams, or even the slab on grade can all provide a rigid backstop for the top and bottom concrete masonry units. These blocks will most likely breakup and will not produce fragments with significant velocities. Removing the top and bottom row of CMU blocks from the fragment calculation aims to account for this behavior. Support configuration for individual walls should be examined, and adjustments should be made accordingly. The figures presented should serve as an illustration of the support blocking phenomenon.

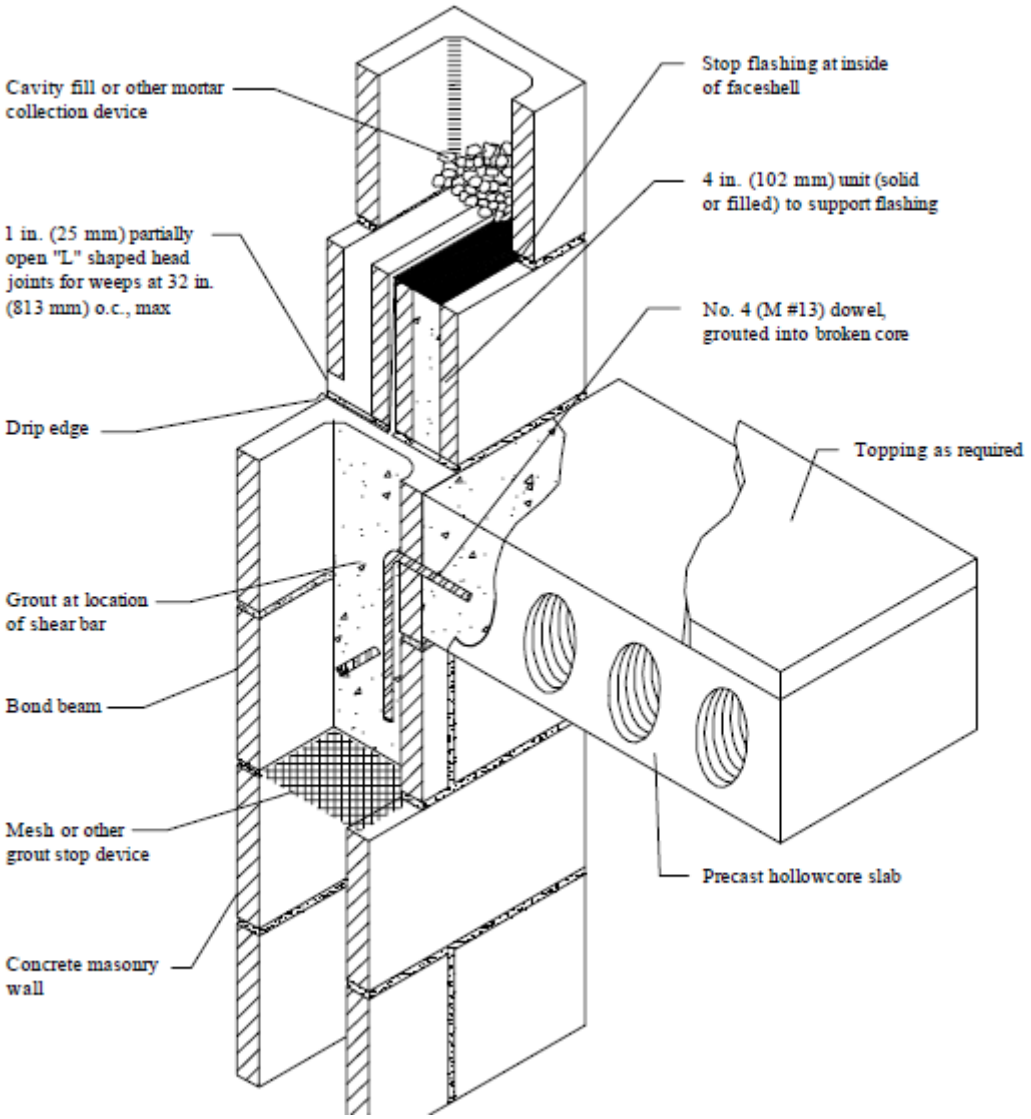

Figure 15: Sidewall Connection 6B.12 (National Concrete Masonry Association 2003)

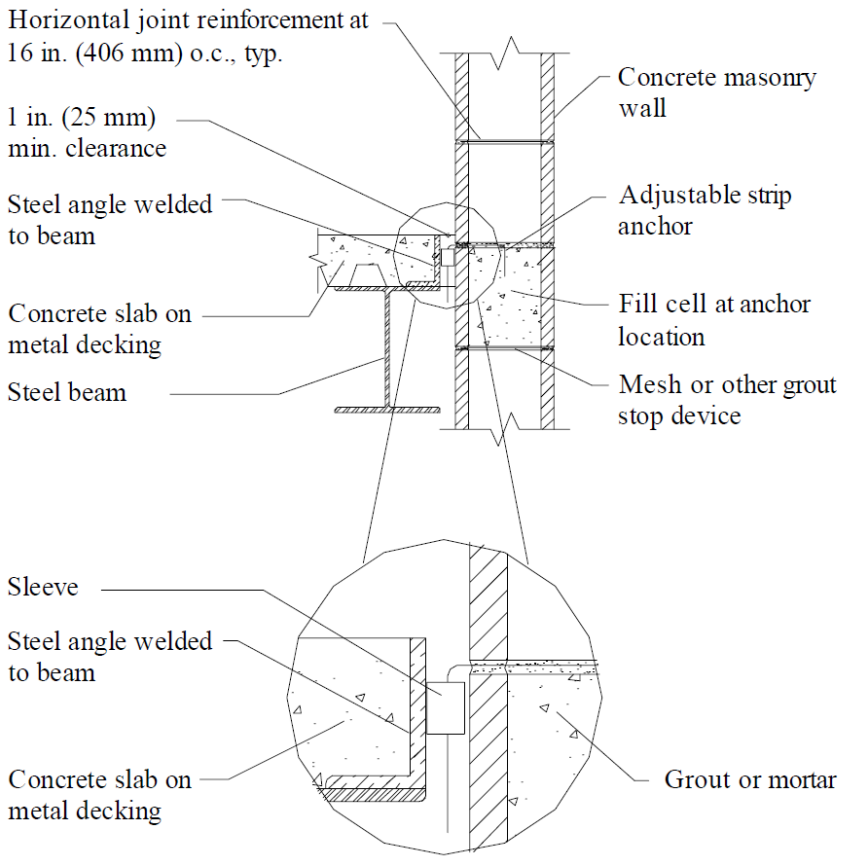

Figure 16 : Steel Beam Connection 3B.4 (National Concrete Masonry Association 2003)

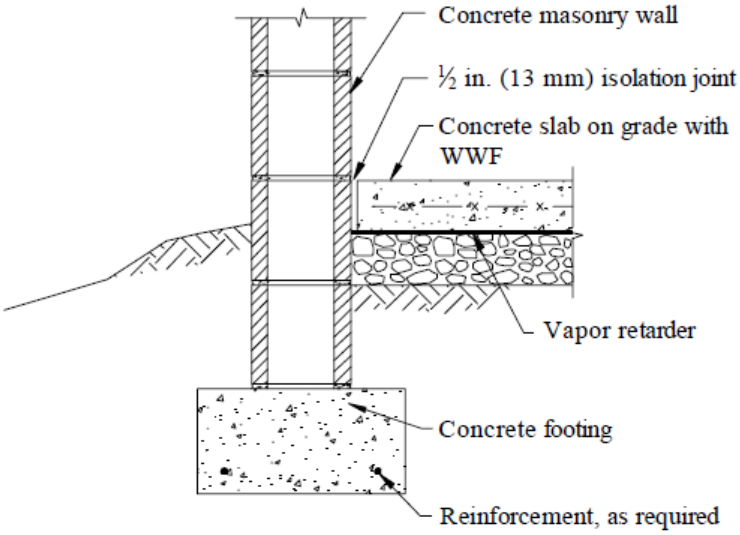

(a) Floating Slab

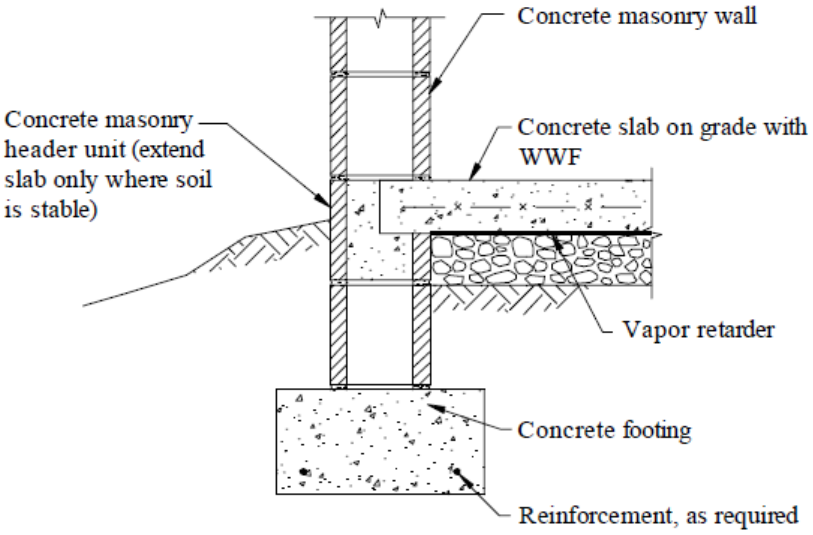

(b) Slab Supported on Header Block

Figure 17: Wall and Slab on Grade Connection 3E.7 (National Concrete Masonry Association 2003)

3.4.3 Strain Energy

The moment of inertia for a one block wide beam bending about its weak axis is given by Equation (3.12). Similarly the cross sectional area for the block is given by Equation (3.13) and shown in Figure 18. These wall parameters can also be found in tabulated forms for given wall configurations.

$$I = \tfrac{1}{12}\left(\ell t_w^3 - \ell_v t_v^3\right) \tag{3.12}$$

$$A_c = \ell t_w - \ell_v t_v \tag{3.13}$$

Where ℓ is the width of the concrete masonry unit (16 in. nominal on a standard block), t_w is the thickness of the unit (8 in. nominal on standard block), ℓ_v is the width of the void, and t_v is the thickness of the void. The wall and block dimensions are treated as if there is no mortar present between the blocks. Ultimately, this results in block dimensions being increased slightly to account for the mortar joints between blocks.

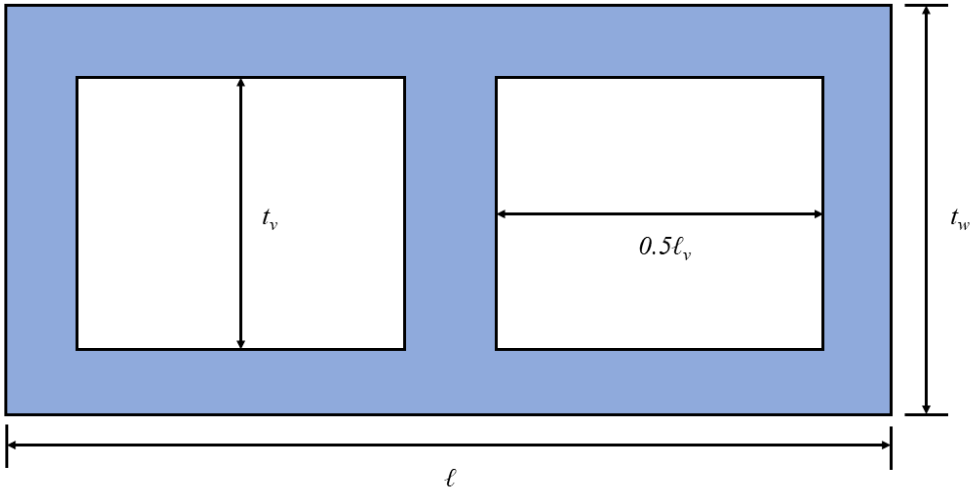

Figure 18: Cross Section of Typical CMU Block

The modulus of elasticity for the concrete masonry units is given by Equation (3.14) found in ACI-318-14 Equation 19.2.2.1.a (American Concrete Institute 2014)

$$E_c = 33 W_u^{1.5} \sqrt{f'_c} \tag{3.14}$$

where E_c is the modulus of elasticity given in psi, W_u is the unit weight of the concrete block material given in pcf, and f'_c is the compressive strength of the unit given in psi. It should be noted that the compressive strength of the concrete masonry unit is only used to calculate the modulus of elasticity and not utilized for any other strength calculations. This f'_c value is the strength of the block material. Note that f'_m, the strength of the CMU and mortar assemblage, is

not used in this calculation. If the f'_m strength is available, then the modulus of elasticity for the masonry assemblage can be used instead of the modulus of elasticity for the blocks only. Equation (3.15) from TSM 402 4.2.2 gives modulus of elasticity for a wall constructed from CMUs

$$E_m = 900 f'_m \tag{3.15}$$

where f'_m is the assemblage compressive strength given in psi (The Masonry Society 2016). This equation is only valid for CMU wall construction. The maximum moment resisted by the unit beam is controlled by the maximum bond stress and any vertical load on the wall. The maximum moment is given by Equation (3.16)

$$M_{\max} = \left(f_r + \frac{P_v}{A_c} \right) \frac{2I}{t_w} \tag{3.16}$$

where f_r is the flexural bond strength, or the flexural tensile strength of the block, whichever is smaller, P_v is the vertical load on the wall, A_c is the cross sectional area of the unit given by Equation (3.13), t_w is the block thickness, Equation (3.12) gives the moment of inertia I. The max moment is related to the applied load by Equation (3.17)

$$M_{\max} = \frac{wL^2}{8} \tag{3.17}$$

where w is the distributed load applied to the unit beam, and L is the length of the beam (height of wall). This relationship only applies to a simply supported beam with a uniformly distributed

load applied to the entire beam length as shown in Figure 9. By combining Equations (3.17) and (3.16) an equation for the maximum resistance of the unit beam can be formulated. Equation (3.2) gives the maximum elastic resistance of a unit beam. A similar formulation is used by Wiehle and Bockholt (1968) to derive their resistance function. Some slight simplifications have been made to the Wiehle and Bockholt (1968) approach to account for the known geometry of a CMU wall.

The elastic strain energy is given by Equation (3.18) (Hibbeler 2014). The equation for the strain energy of a beam in bending is

$$E_{strain1} = \int_0^L \frac{M(x)^2}{2EI} dx \tag{3.18}$$

where *M(x)* is the moment along the beam, *L* is the length of the unit beam (height of wall), *E* is the modulus of elasticity for the concrete masonry units, and *I* is the moment of inertia of the unit beam. The formulation for *M(x)* in terms of the applied loading is given by Equation (3.19).

$$M(x) = \frac{wx}{2}(L - x) \tag{3.19}$$

where *w* is the uniformly distributed loading, *L* is the height of the wall, and *x* is the distance along the wall measured from one end.

Finally Equation (3.18) can be combined with Equations (3.1) and (3.19) to give Equation (3.20). This gives the strain energy absorbed by the unit beam as it deflects until failure. Note that this equation must be modified for different support conditions.

$$E_{strain1} = \frac{1}{240}\frac{w^2 L^5}{EI} = \frac{1}{240}\frac{Q_1^2 L^3}{EI} \tag{3.20}$$

A methodology similar to the one used for the elastic strain energy calculation was used to calculate the secondary strain energy. The aim of this methodology was to calculate a mechanically consistent and accurate value for the secondary strain energy. A diagram of the physical situation is displayed in Figure 10, and the relationship between the resistance and deflection can be seen in Figure 19.

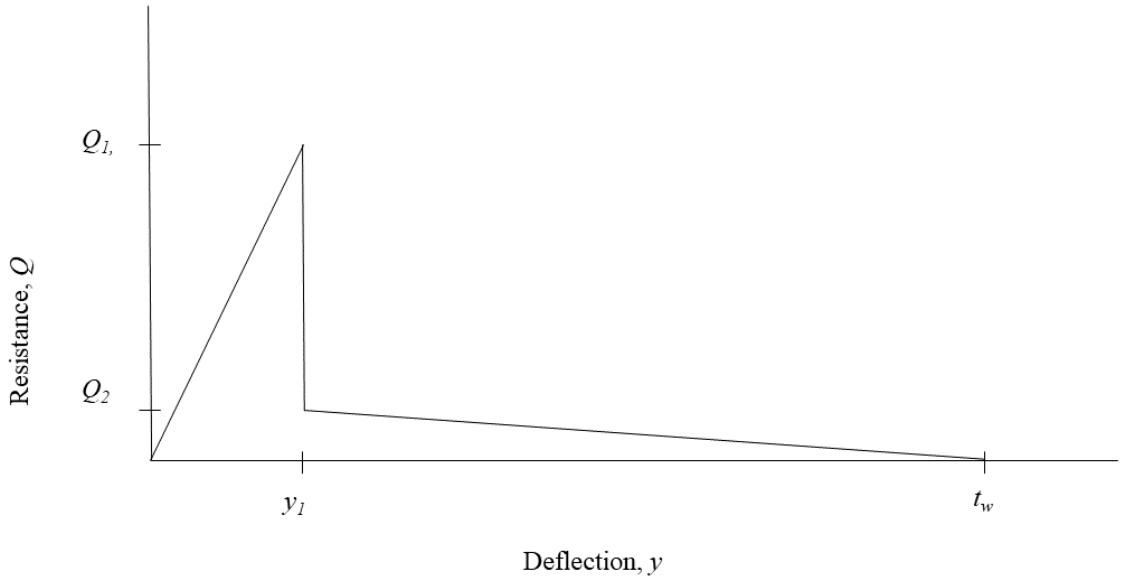

Figure 19: Resistance and Deflection Plot for Secondary Resistance Calculation

This equation gives the work required to move each differential segment of the wall a distance y.

$$E_s = \tfrac{1}{2} F y \tag{3.21}$$

where E_s is the energy F is the applied force and y is the deflection. The force at any given point along the height of the wall is given by Equation (3.22) and the distance that section moves is given by Equation (3.23) where x is measured vertically from the top of the wall to the center of the wall. The deflection of the half beam section is shown in Figure 20.

$$F = (w)dx \tag{3.22}$$

$$y = \frac{2x}{L}(t_w - y_1) \tag{3.23}$$

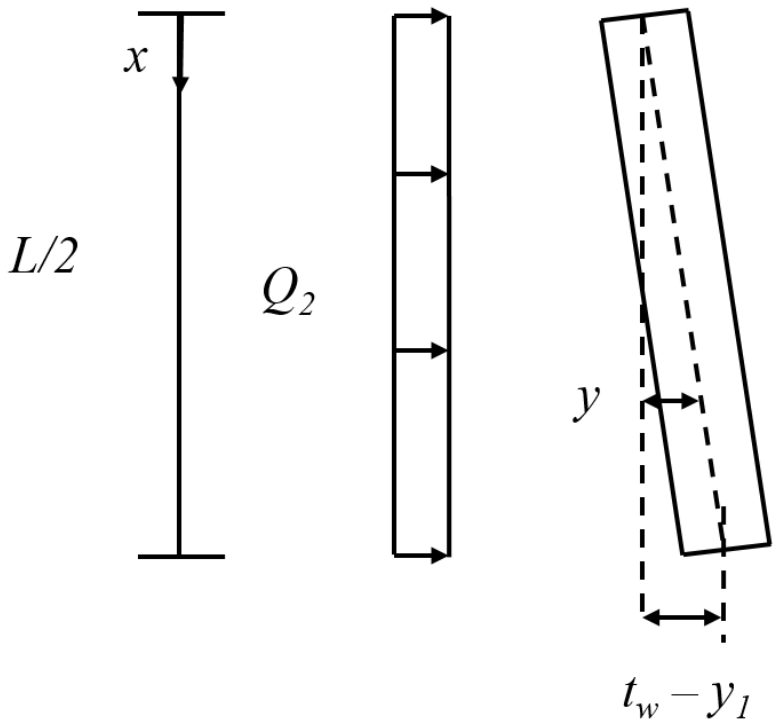

Figure 20: Top Half Beam Section Deflection

Substituting Equation (3.22) and (3.23) into Equation (3.21) yields the Equation (3.24), which gives the strain energy of a wall segment with height *dx* along the wall after it has deflected through the entire secondary resistance phase. Figure 21 shows the differential element at a distance *x* from the top support.

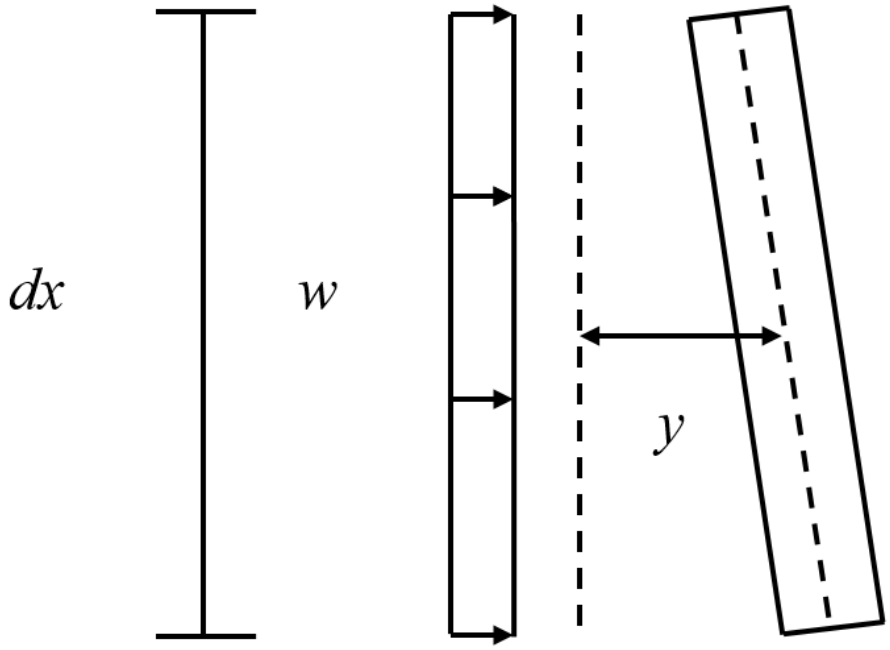

Figure 21: Differential Beam Element

If Equation (3.24) is integrated from zero to the center of the wall then it gives the strain energy for one half of the wall which is given by Equation (3.25). That value is then multiplied by two to give the strain energy for the entire wall, Equation (3.26).

$$E_s = \frac{wx}{L}(t_w - y_1)dx \tag{3.24}$$

$$\tfrac{1}{2}E_T = \int_0^{L/2} \frac{wx}{L}(t_w - y_1)dx \tag{3.25}$$

$$E_{strain2} = \tfrac{1}{4} Q_2 (t_w - y_1) \tag{3.26}$$

where Q_2 is the maximum secondary resistance given by Equation (3.4), t_w is the thickness of the wall, and y_2 is the elastic displacement given by Equation (3.3). The strain energy from the secondary resistance is given by Equation (3.26). This is the energy required to rotate the top and bottom half of the wall until they become unstable at one wall thickness of mid-height deflection. Both strain energy absorption mechanisms have been defined, the total strain energy absorbed by the wall is given by Equation (3.27).

$$E_{strain} = E_{strain1} + E_{strain2} \tag{3.27}$$

3.4.4 Kinetic Energy

The final term in Equation (3.8) is the kinetic energy term. The kinetic energy can be calculated by rearranging Equation (3.8) to solve for the unknown kinetic energy term

$$E_{ke} = E_{in} - E_{strain} \tag{3.28}$$

Where E_{ke} is the kinetic energy of the entire wall, E_{in} is the energy input into the wall, and E_{strain} is the amount of energy the wall absorbs as it deflects.

The strain energy calculation employs a static resistance function. No dynamic effects were incorporated into the strain energy formulation. Modifications to account for changes in strain energy due to dynamic loading were explored, but no serviceable modification methodology was deemed acceptable. It was reasonable to assume that the dynamic strain energy

absorbed by the member would be greater than the static value. Kinetic energy predictions without any dynamic modifications were reasonable so any dynamic effects should be relatively small. However, a more robust dynamic strain energy definition can only improve predictions and may be more important for different wall configurations.

Equation (3.29) gives the total kinetic energy of the entire wall. It is assumed that the energy is distributed evenly over the entire wall. This assumption can be combined with the assertion that each fragment has a uniform size. Thus, the kinetic energy of each individual fragment is equal and can be given by Equation (3.29)

$$e_{ke} = \frac{E_{ke}}{n_b} \tag{3.29}$$

where e_{ke} is the kinetic energy of each **individual** fragment or block, and n_b is the total number of blocks or fragments in the wall being examined. The relationship between the kinetic energy of a body and its velocity is given by Equation (3.30). This can be rearranged to solve for velocity and gives Equation (3.31)

$$e_{ke} = \tfrac{1}{2} m v^2 \tag{3.30}$$

$$v = \sqrt{\frac{2e_{ke}}{m}} \tag{3.31}$$

where e_{ke} is the kinetic energy, m is the mass of a single block, and v is the velocity of a single block. The velocity generated by this calculation is an aggregate value. It is likely that some

fragments travel with more velocity and some with less velocity. A single velocity value results from assuming the fragments are all uniform in size and that energy is distributed evenly over the entire wall. These assumptions apply within the limitations of the presented methodology.

Testing efforts that generate wall velocities generally only produces a few velocity data points per wall. The velocity readings are produced by accelerometers or displacement gauges attached to the wall at discrete points. It is not feasible to mount an accelerometer on every single block in a test wall. Instead, a small number of strategically located accelerometers are usually placed along the vertical center of the wall. Wall velocity, along the vertical axis, seems to be generally uniform. Relatively uniform wall velocities were observed during both validation testing efforts.

3.5 Strain Energy Comparison

While searching for an effective way to formulate the stain energy of a dynamically loaded beam, alternate methods for determining the elastic strain energy ($E_{strain1}$) were explored. Using the Wiehle and Bockholt (1968) method to formulate the resistance function for the wall, a deflection and resistance function was created. The area under this force versus deflection curve was assumed to be a good estimation of the strain energy. By operating under similar assumptions and methodologies to those presented in Section 3.4.3 Strain Energy, the alternate elastic strain energy can be calculated by Equation (3.32).

$$E_{strain1} = \frac{5}{768}\frac{Q_1^2 L^3}{EI} \tag{3.32}$$

This methodology for calculating the strain energy results in a slightly larger value for the strain energy when compared to the value calculated by Equation (3.20). The more rigorous method for calculating strain energy (via Equation (3.20)) was used in this methodology because it provided a smaller value for the strain energy. The smaller strain energy value resulted in larger kinetic energy predictions. Higher kinetic energy predictions for wall fragments were deemed to be conservative because they resulted in larger predicted velocities. This alternate method for calculating the strain energy by Equation (3.32) only required the adoption of an accurate resistance definition. For the current effort the more rigorous method of calculating strain energy by integration was not very difficult since the mechanics of the system were well defined. However, future efforts with more complicated support conditions or complex constitutive relationships may not be able to easily formulate the strain energy using the more rigorous approach. In these cases, it may be acceptable to formulate the strain energy directly from the resistance function as illustrated above.

The difference between the rigorous elastic strain energy formulation of Equation (3.20) and the force versus displacement formulation of Equation (3.32) results from discrepancies between the mechanical assertions of both formulations. The rigorous formulation takes an integral of the strain energy over the entire beam, which accounts for the curvature of the beam due to loading. As the beam deflects, the load near the supports does not displace as much as the load at the midspan. By integrating the strain energy over the entire height of the wall in Equation (3.20) the variation in displacement was accounted for. Conversely, the force vs. displacement method does not account for this displacement variation. It simply displaces the

entire distributed load as a point force through the total midspan displacement. The strain energy is overestimated because the total force is displaced through the midspan deflection. In the Equation (3.20) formulation each portion of the distributed force is moved through the assumed displacement it experiences during wall loading. This formulation results in a more accurate approximation of the strain energy absorbed by the wall during deflection.

Similarly, different methods were explored for calculating the strain energy absorbed during the secondary resistance phase. One method proposed was to simply calculate the area under the secondary resistance curve. The main advantage of this method was the simplicity of the calculation. As stated before, this may still be a viable method for more complicated loading behavior or wall configurations. Equation (3.33) gives the strain energy for the secondary curve area method.

$$E_{strain2} = \tfrac{1}{2} Q_2 (t_w - y_2) \tag{3.33}$$

This gives twice the secondary strain energy of Equation (3.26). Ultimately, this formulation was not used because it gave a larger value for the strain energy. Again, the entire applied force on the wall is moved through the maximum wall displacement, which resulted in a larger strain energy approximation. The more rigorous method of Equation (3.26) gave a smaller value because it accounted for the different displacements of each distributed load along the entire height of the wall. The Equation (3.26) method was a more accurate approximation of the strain energy of the secondary resistance phase so it was used in the current effort.

3.6 Utilizing Energy Formulation for Wall Failure Criteria

Because of the low strength of a URN CMU wall when loaded out of plane, the strain energy absorbed during deflection is quite small compared to the energy input by most airblast loads. Most of the input energy is converted directly to kinetic energy. This confirms what has been experimentally observed: unreinforced concrete masonry walls are inherently weak to blast loading (Baylot et al. 2005; Gagnet 2013). However, there are potential reflected pressure loads that will not cause an UNR CMU wall to fail.

If the input energy is greater than the strain energy, the wall fails, and its fragments have some residual kinetic energy. However, if the input energy is less than or equal to the strain energy then the wall will not fail. The inequality matrix given by Equation (3.34) illustrates this idea. The failure criteria illustrated here arise from the rigid enforcement of an energy balance formulation.

$$\begin{aligned} E_{strain} < E_{in} &\rightarrow Fail \\ E_{strain} \geq E_{in} &\rightarrow NonFail \end{aligned} \tag{3.34}$$

There is a small range of input energies that result in no wall failure. The degree of partial wall failure cannot be reliably predicted from this methodology. Wall fragments should exhibit no inward (towards building occupants) traveling velocities when inside this range of input energies. An outward or negative velocity prediction simply indicates that the strain energy absorption potential is greater than the energy imparted to the system. Fragments may experience a negative or outward velocity in this state, but no effort to predict this behavior is undertaken

here. The only assertion that the current methodology makes about this response state is that significant inward (positive) fragment velocities should not occur. In summary, if the energy imparted to the wall is lower than the total energy absorption potential of the wall, fragments with inward velocities should not be produced.

If the input energy is less the strain energy, the model asserts that wall fragments do not travel inward. It is possible that the wall may be damaged enough where it provides little protection or collapses, but it should not produce fragments with meaningful positive velocities. The range of input energies that produce this behavior is quite small, but not negligible.

At larger input energies, the amount of energy absorbed by the wall is almost negligible compared to the energy imparted to the wall. For these walls, the kinetic energy of the fragments is almost solely defined by the amount of energy imparted to the wall by the reflected pressure wave. However, at lower input energies, the wall absorption energy has a significant impact on the residual kinetic energy. For low energy airblasts it is critical to model the absorption energy correctly.

Attempts were made to modify the strain energy with a constant multiplier. This is shown in Equation (3.35).

$$\begin{aligned} \alpha E_{strain} < E_{in} &\rightarrow Fail \\ \alpha E_{strain} \geq E_{in} &\rightarrow NonFail \end{aligned} \tag{3.35}$$

The aim of the constant α was to increase the energy range where no fragment predictions were made. This would help to reflect the uncertainty surrounding any velocity prediction near this

failure point energy. Multiplying this failure point energy by an alpha value greater than one created a “buffer zone” around the failure point where no velocity prediction was made and no prediction about the failure or non-failure state of the wall was undertaken. The secondary aim of the alpha modifier was to help account for dynamic effects by increasing the strain energy absorbed by the wall. However, no mechanical defense could be formulated for the utilization of the alpha modifier. Therefore, it was removed.

For any given wall and input loading combination, there will be many impulse values that produce significant positive fragment velocities. Selecting the appropriate impulse value along the duration of the loading event for velocity prediction and wall failure prediction is imperative. The free flight velocity was the goal of this methodology, so the impulse value at the end of the negative phase was used for predictions.

Chapter 4: Predicting the Pressure Time History

To utilize the methodology presented in this effort effectively, the impulse-time history and subsequently the pressure-time history must be either known or accurately predicted. The Friedlander fit is a well-accepted method for predicting the positive pressure phase (Friedlander 1940). Additionally, there are multiple methods presented in the literature that attempt to predict the negative pressure time history. Rigby et al. (2014) summarized and examined three major methods of negative phase prediction and presented their own prediction method.

Rigby et al. (2014) conducted a review and comparison of three major prediction methods with their own. The Linear Approximation method presented by Krauthammer and Altenberg (2000) models the negative phase as a simple triangle. The rise time is equal to one quarter of the duration of the total negative phase. The total impulse and minimum pressure of the negative phase is given by the blast parameters presented in the UFC 3-340-02 (Department of Defense 2008). This method is recommended in the UFC 3-340-02. The Extended Friedlander method was presented by Dharani and Wei (2004) and simply extends the Friedlander equations for the entire duration of the blast loading. This encompasses both the positive pressure phase and negative pressure phase. Finally, the prediction method conceived by Teich and Gebbeken (2010), is a modified Friedlander extension termed "Extended Friedlander with Teich C_r^-". This method sought to improve the Extended Friedlander prediction by modifying the negative phase pressure equation with a scaling parameter. The goal of this effort was to make the predictions for negative impulse more closely match the blast parameters presented in the UFC 3-340-02.

The prediction method presented by Rigby et al. (2014) models the negative phase as a cubic expression. The cubic expression that Rigby uses was originally utilized by Granström (1956). The cubic method from Rigby uses the minimum pressure and negative impulse parameters given by UFC 3-340-02 to determine the predicted negative phase duration such that the cubic predicted impulse matches the negative impulse given by UFC 3-340-02. The predicted negative phase pressure has the same minimum pressure and negative impulse as predicted by the UFC 3-340-02 parameters. The negative phase duration is adjusted so that the cubic equation has the desired parameters.

The four prediction methods described above were examined and compared to test data by Rigby et al. (2014). Figure 22 shows the relationship between the four different prediction methods presented by Rigby.

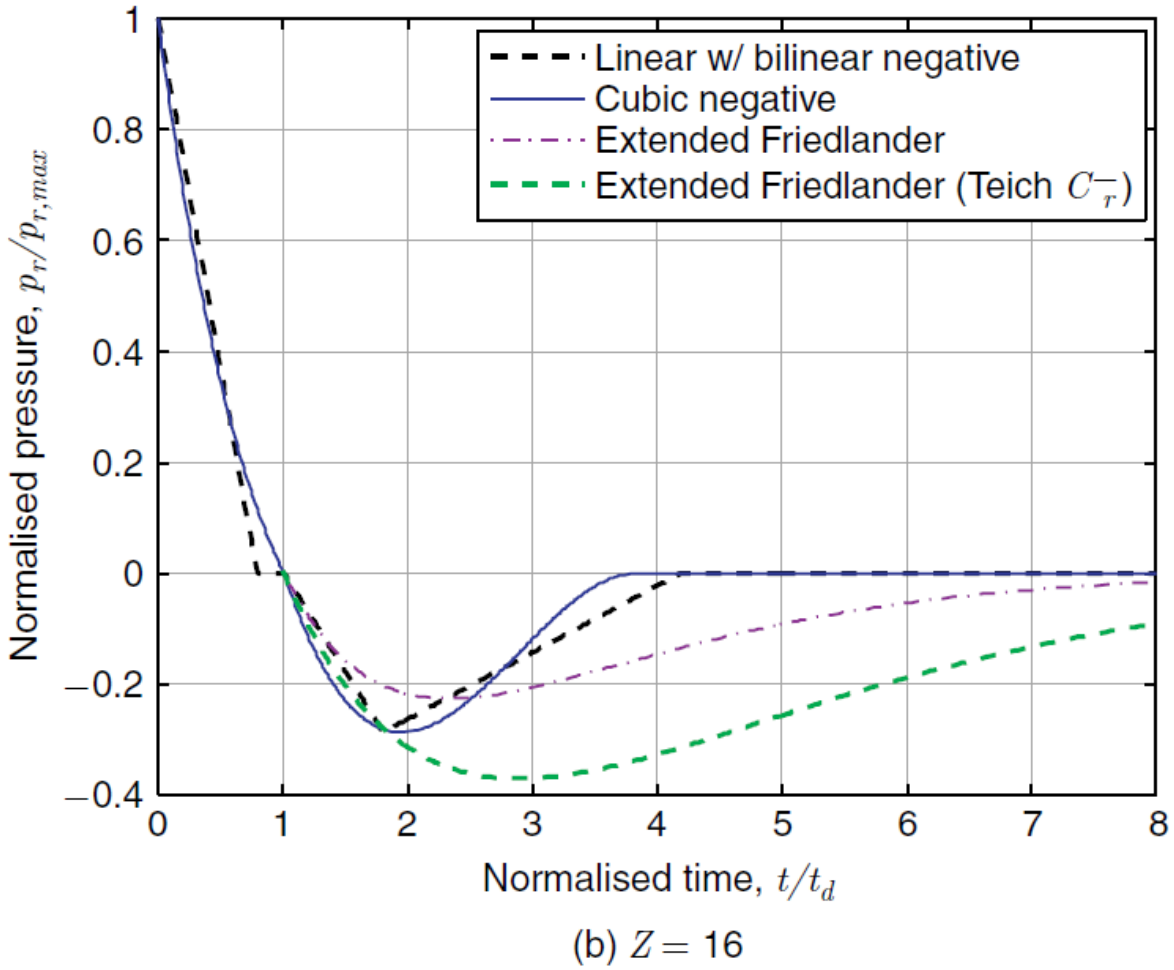

Figure 22: Comparison Between Negative Phase Prediction Methods at Z=16 (Rigby et al. 2014)

Figure 23 shows the different prediction methods plotted with four different negative phase reflected pressure time histories generated via testing. Rigby et al. (2014) generated an observed reflected pressure time history at four different scaled distances and compared their prediction method with the prediction methods discussed above. The tests were conducted at the University of Sheffield Blast & Impact Laboratory, Buxton, UK. A large reinforced concrete bunker was used to provide a relatively rigid target. The experimental work and subsequent

analysis conducted by Rigby et al. (2014) was used as a basis for excluding the other three prediction methods presented as potential approaches for predicting the total reflected negative phase impulse.

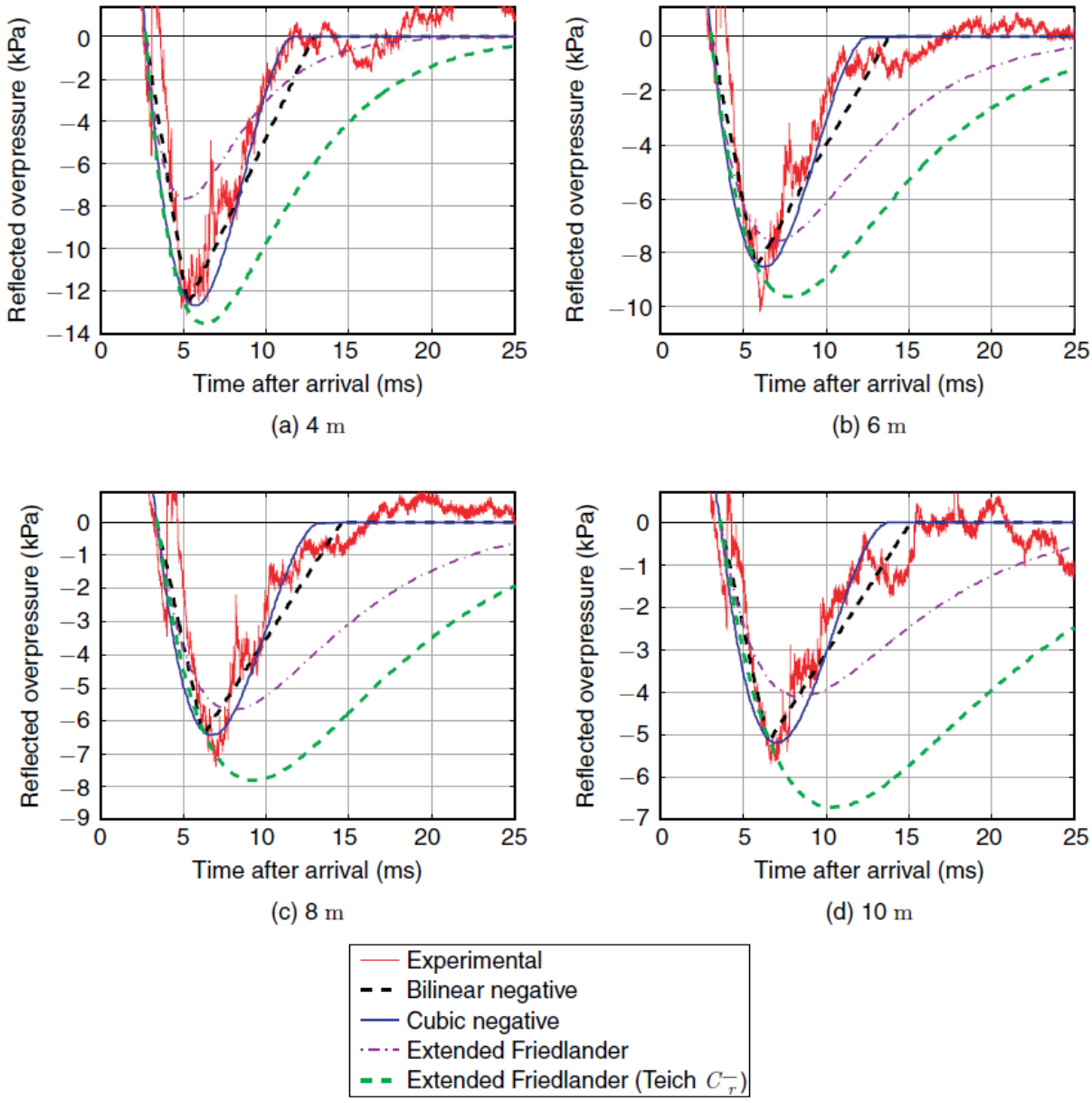

Figure 23: Experimental and Predicted Negative Phase Pressure Time Histories (Rigby et al. 2014)

Initially, the Rigby et al. (2014) method was utilized to predict the negative phase blast pressure-time history; however, when the prediction method was compared to the available test data there were large discrepancies between the observed data pressure-time history and the predicted pressure time history. Figures 24-29 show the large differences between the predicted pressure time history via the Rigby et al. (2014) prediction method and the observed reflected pressure time history. It should be noted that, only the reflected negative phase pressure time history is displayed. Figure 24 and Figure 25 show the reflected pressure-time history for the ERDC full-scale test, and Figure 26 through Figure 29 show the reflected pressure time history for the TSWG quarter-scale tests. The details of how these observed reflected pressure time histories were obtained will be addressed in Chapter 5: Comparison and Validation. Note that these pressure time histories were normalized based on the maximum reflected pressure for each test and total duration.

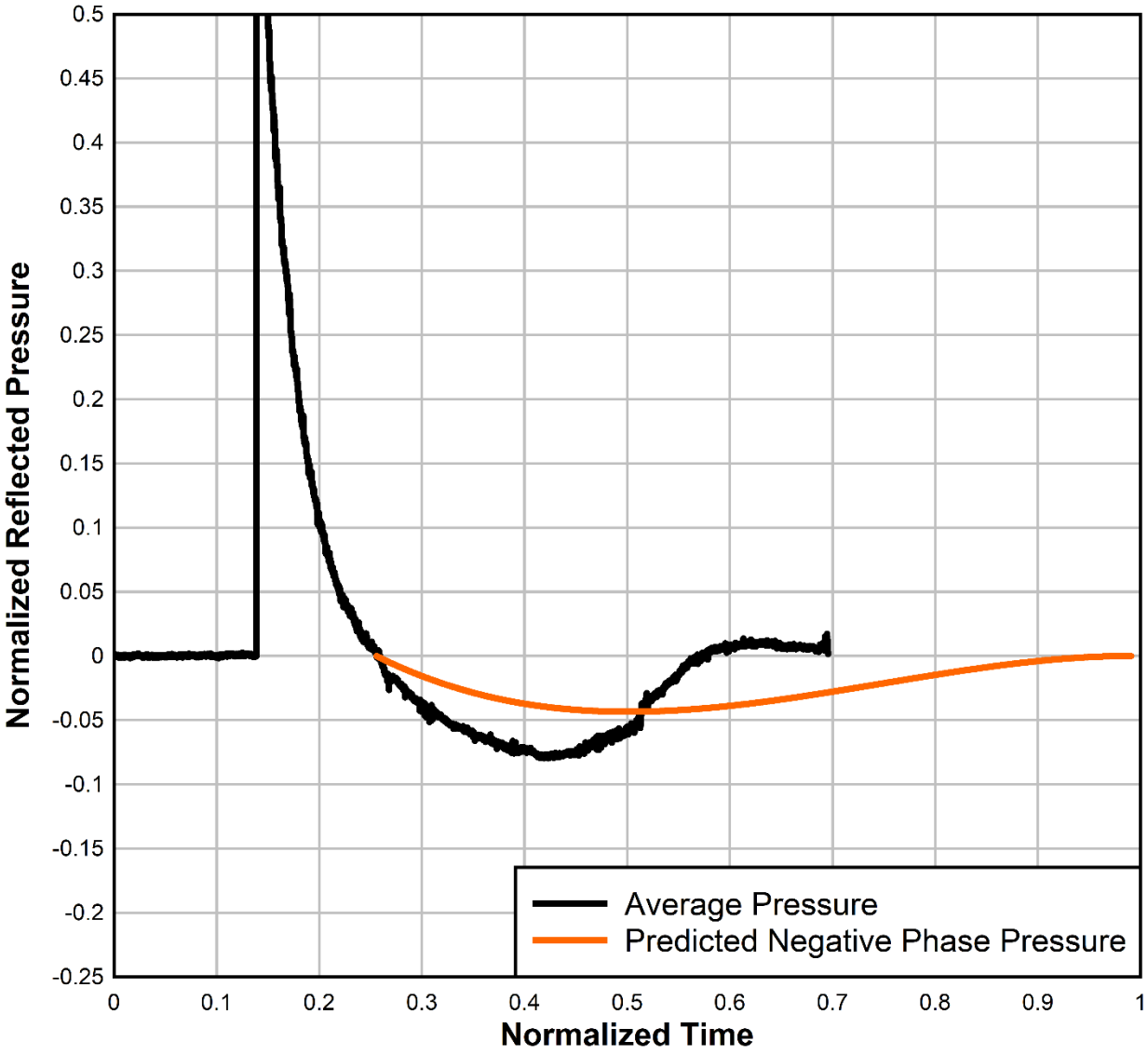

Figure 24: Rigby Prediction and Experimental Pressure Time History Full-Scale Test 1

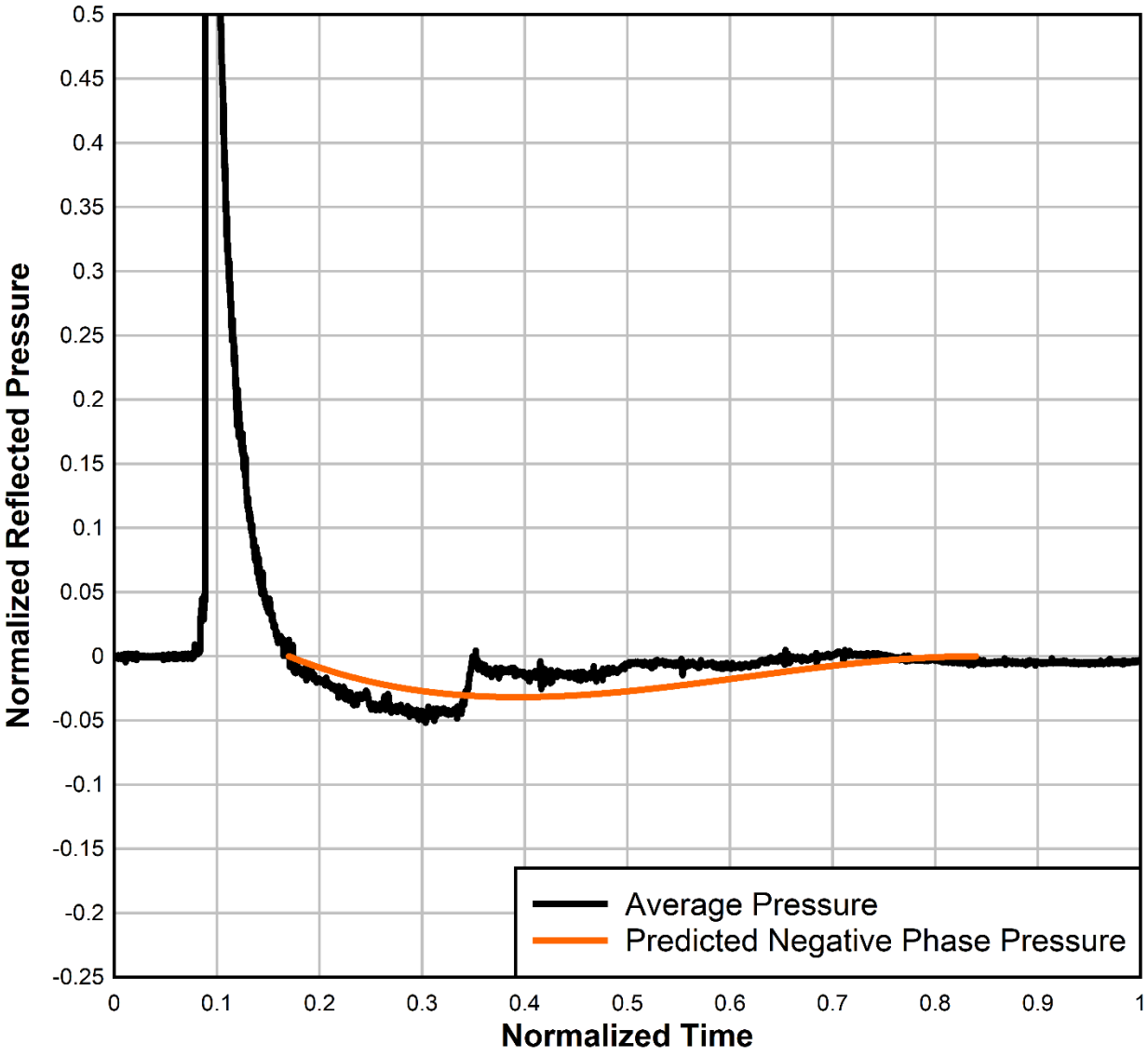

Figure 25: Rigby Prediction and Experimental Pressure Time History Full-Scale Test 2

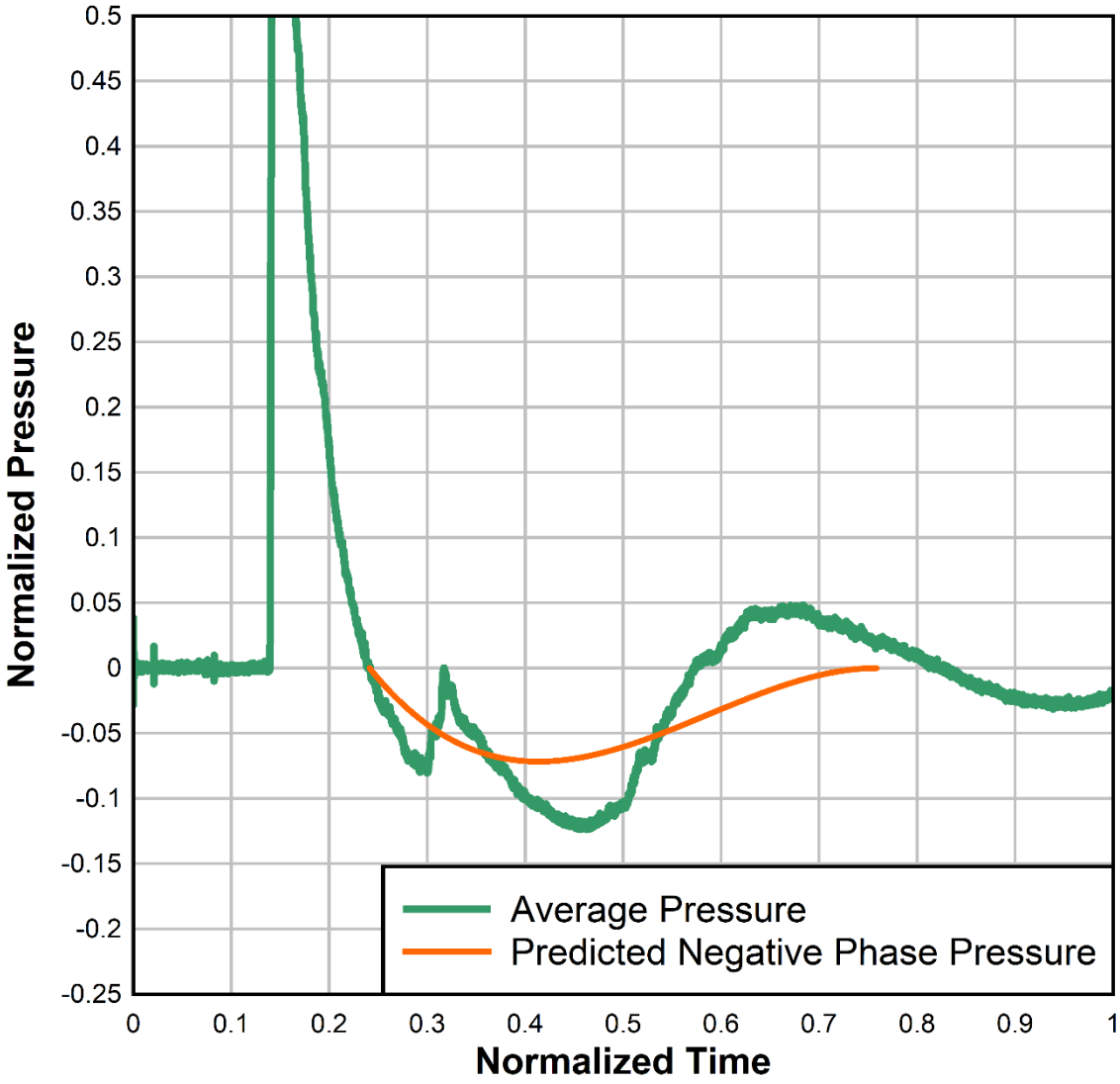

Figure 26: Rigby Prediction and Experimental Pressure Time History Quarter-scale Test 1

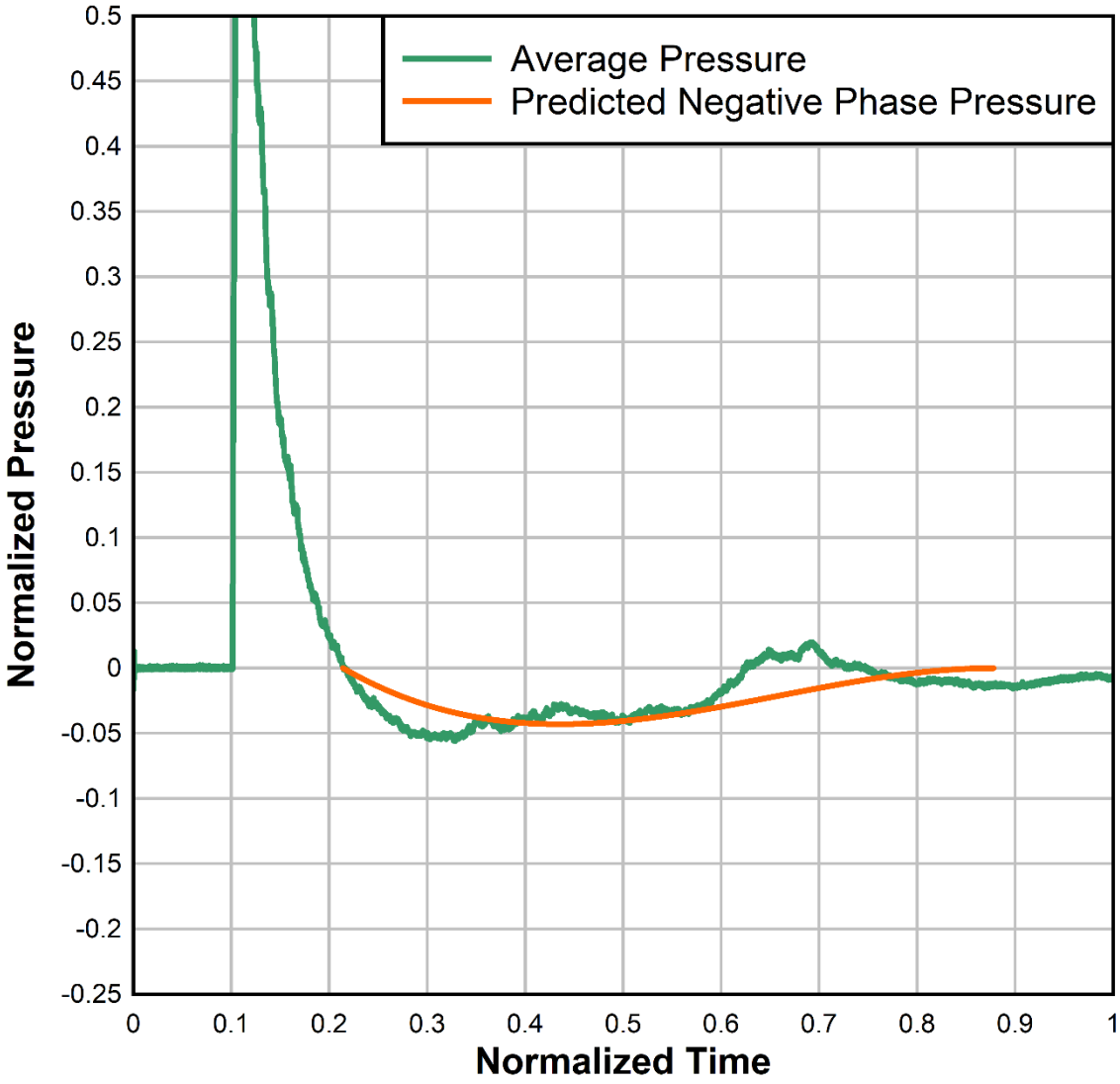

Figure 27: Rigby Prediction and Experimental Pressure Time History Quarter-scale Test 2

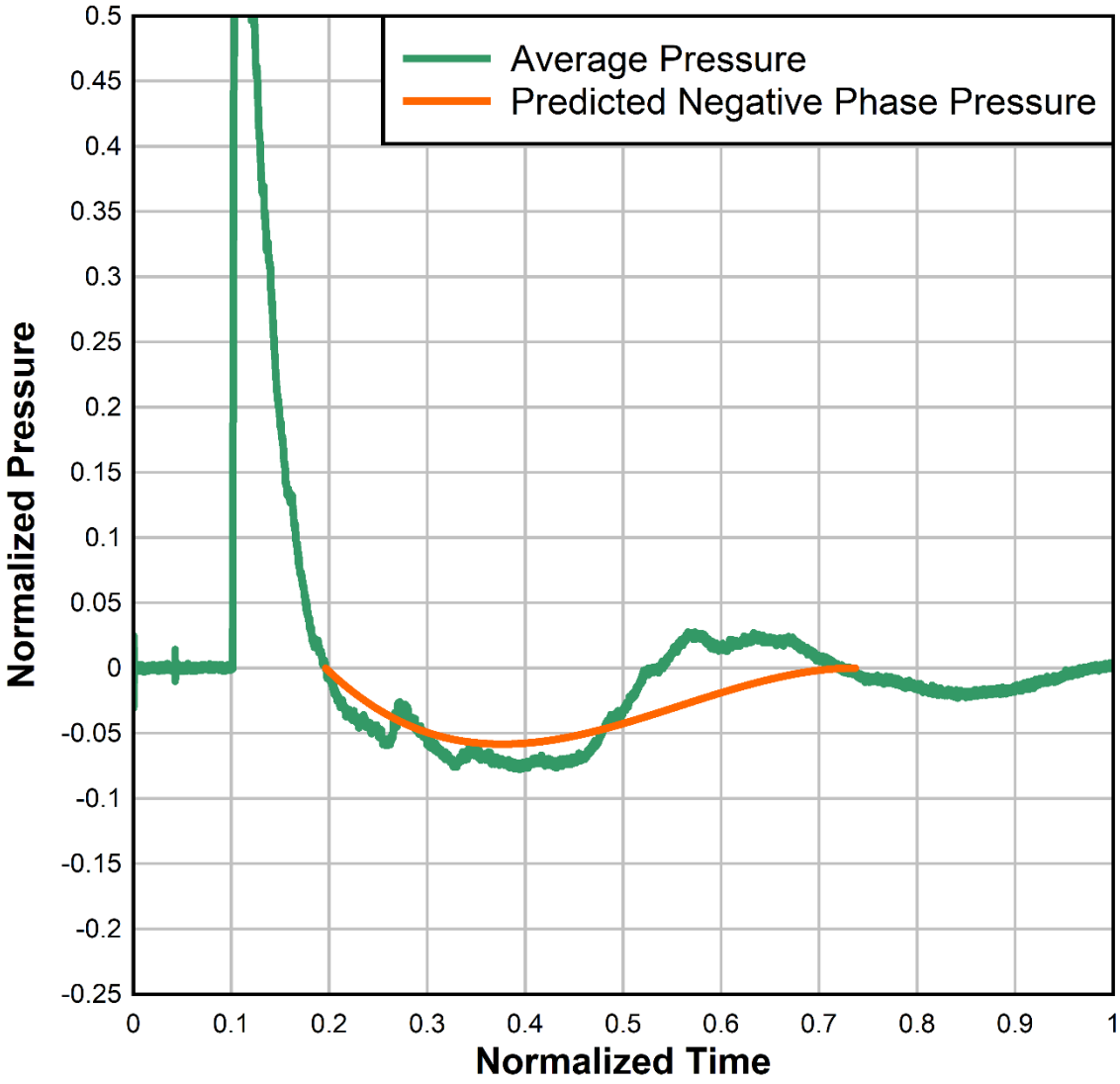

Figure 28: Rigby Prediction and Experimental Pressure Time History Quarter-scale Test 3

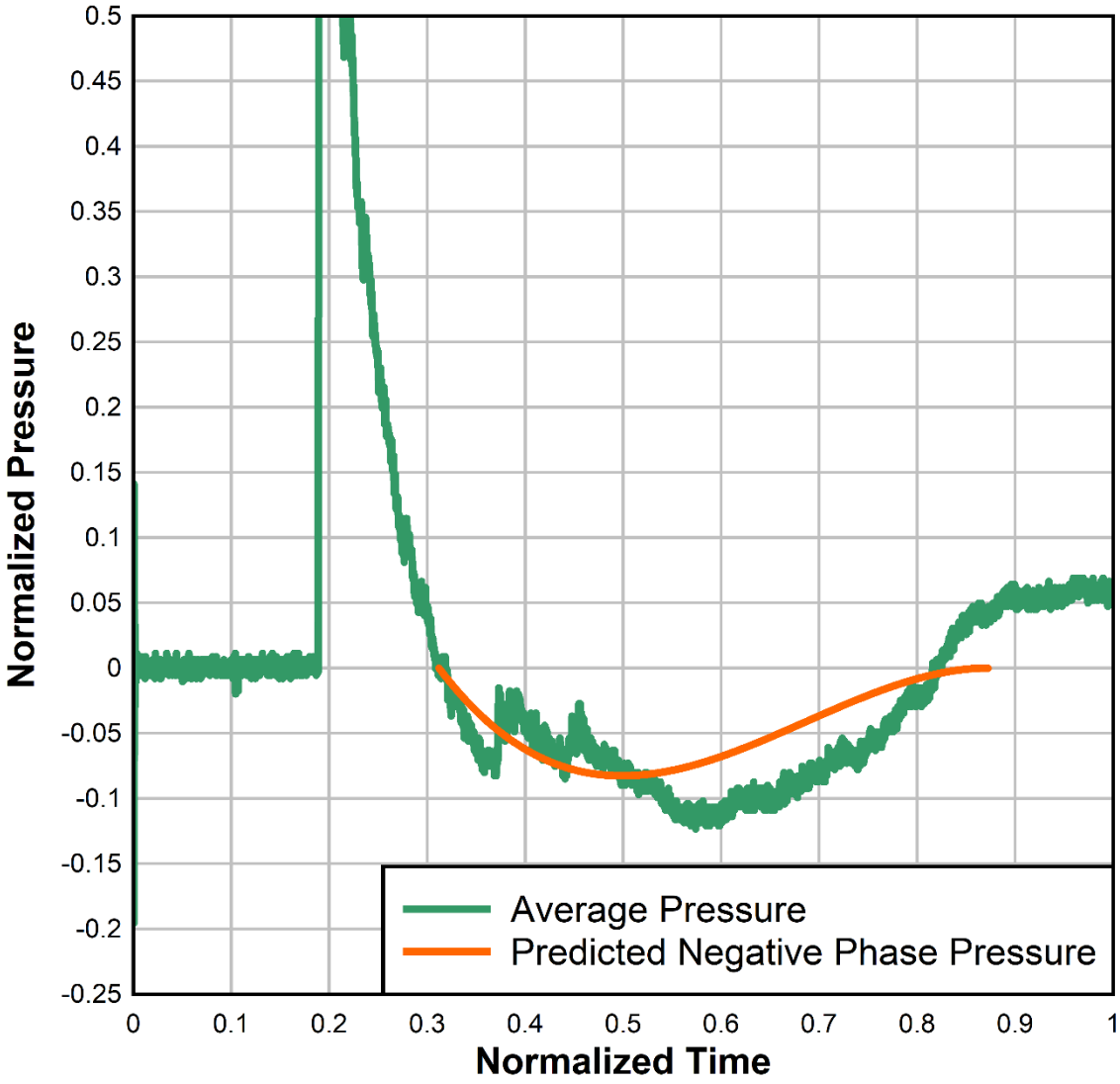

Figure 29: Rigby Prediction and Experimental Pressure Time History Quarter-scale Test 4

Ultimately, this prediction method applies the negative phase blast parameters presented in the UFC 3-340-02 and creates a smooth cubic curve pressure time history that matches the minimum pressure and negative phase impulse blast parameters. The predicted negative phase duration is significantly longer than the observed duration for the ERDC and TSWG experiments, and the predicted magnitude of the reflected negative pressure is less than the observed reflected pressure.

The observed negative phase pressure time histories do not match the prediction parameters presented in the UFC 3-340-02. It is possible that the secondary shock phenomenon skewed the data resulting in this discrepancy. The secondary shock phenomenon seemed to be more evident in the full-scale testing when compared to the quarter-scale data. The pressure-time history prediction matched the quarter-scale more closely than the full-scale data. Secondary shock may account for the low impulse, minimum pressure, and duration, but the evidence is inconclusive.

Interestingly, secondary shock seemed to have very little impact on the data presented by Rigby et al. (2014). Secondary shock was observed in their data, it occurred significantly earlier than was observed in the full-scale and quarter-scale experiments. It effectively started before the negative phase had even initiated. Figure 30 shows an annotated typical reflected pressure time history that Rigby et al. (2014) presents. This negative phase seems to be typical of all the other pressure time histories that are presented in the Rigby examination. The secondary shock occurs very early on in the negative phase which means it simply delays the onset of the negative phase loading by 1 to 2 milliseconds. Conversely, for the test data presented in this effort, the onset of the secondary shock phenomenon was much later and larger in magnitude. The secondary shock occurred after the onset of the negative phase for the ERDC full-scale data much later than observed in the Rigby examination. The quarter-scale TSWG tests have a less defined secondary shock that is significantly less in magnitude. It is possible that the secondary shock phenomenon is the cause for the discrepancy between the data presented by Rigby et al. (2014) and the data collected in this effort. However, these conclusions are tentative and based on limited data and should serve only as a guide to future research on the subject. The negative phase discrepancy

examination was included in this effort as a justification for the lack of a negative phase prediction methodology being implemented in the current effort.

Ultimately, the discrepancies between the observed data and the proposed prediction method were too large to allow for the useful prediction of the negative phase reflected pressure time history. Therefore, the current effort must rely on experimentally observed reflected pressure time histories. Once an effective method for predicting the negative phase pressure time history becomes available, it should be used in conjunction with this prediction methodology to provide accurate fragment velocity predictions.

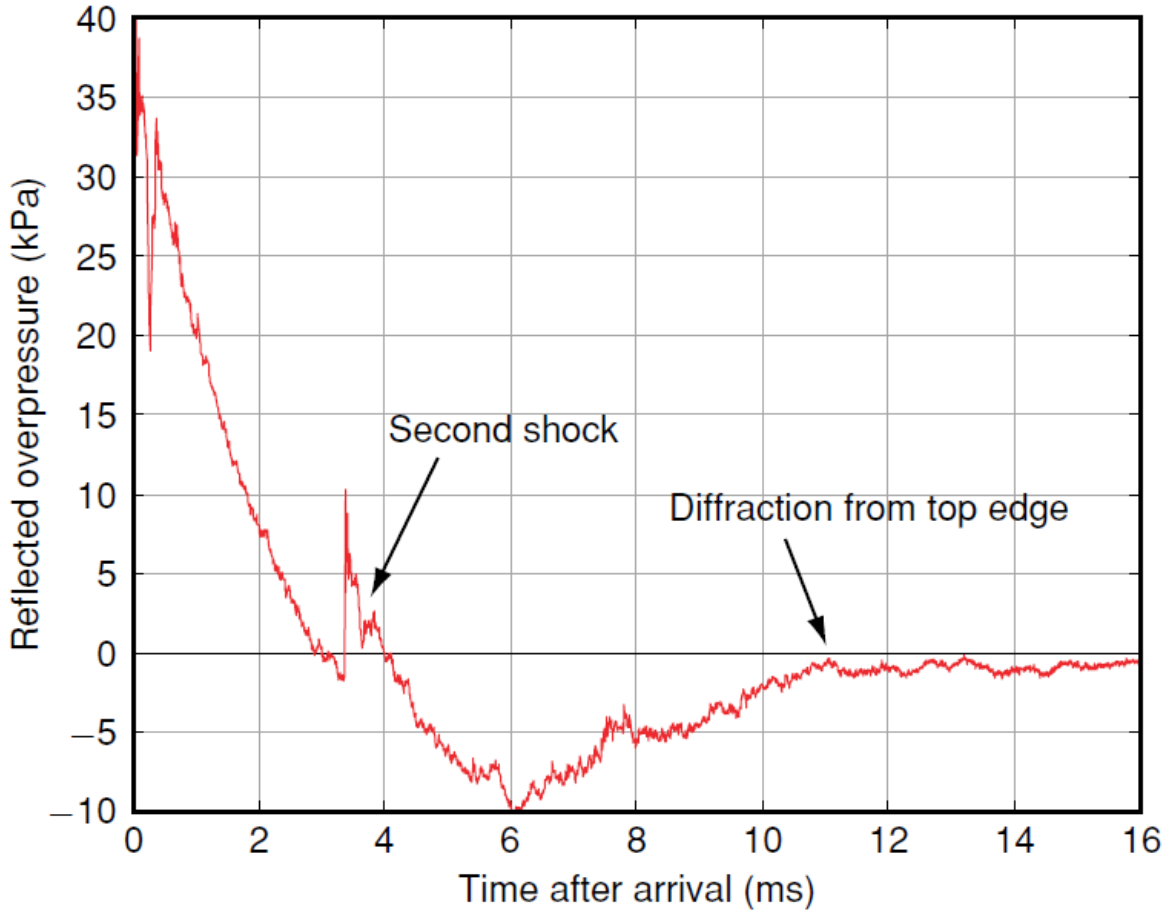

Figure 30: Annotated Pressure Time History (Rigby et al. 2014)

This area of blast research needs to be examined more closely. The subject of secondary shock seems to be more important than previously thought. Additionally, it is possible that the negative phase blast parameters presented in the UFC 3-340-02 should be revisited. Attempts were made ascertain the origin of these parameters. No definitive answer was reached. However, it seems possible that the basis for these parameters was presented by Granström (1956). Or at the very least, the same data they examined was also used separately for the derivation of the UFC 3-340-02 parameters. The plot Granström (1956) presented is similar in shape to the ones presented in the UFC 3-340-02. Figure 31 shows the pressure vs scaled distance plot presented

by Granström (1956). The predictions presented here are based on three separate experiments referenced by Granström (1956, p. 57). The first was conducted by Criborn in 1948 and utilized a “corona microphone indicating static pressure” to record pressure values. The second was done by Bernal in 1940 and “probably [used] piezo-electric measurements, method not specified” to get pressure data. Finally, Ritter in 1925 used a “membrane gauge with mechanical recorded, probably indicating approximate reflection pressure” to generate test data.

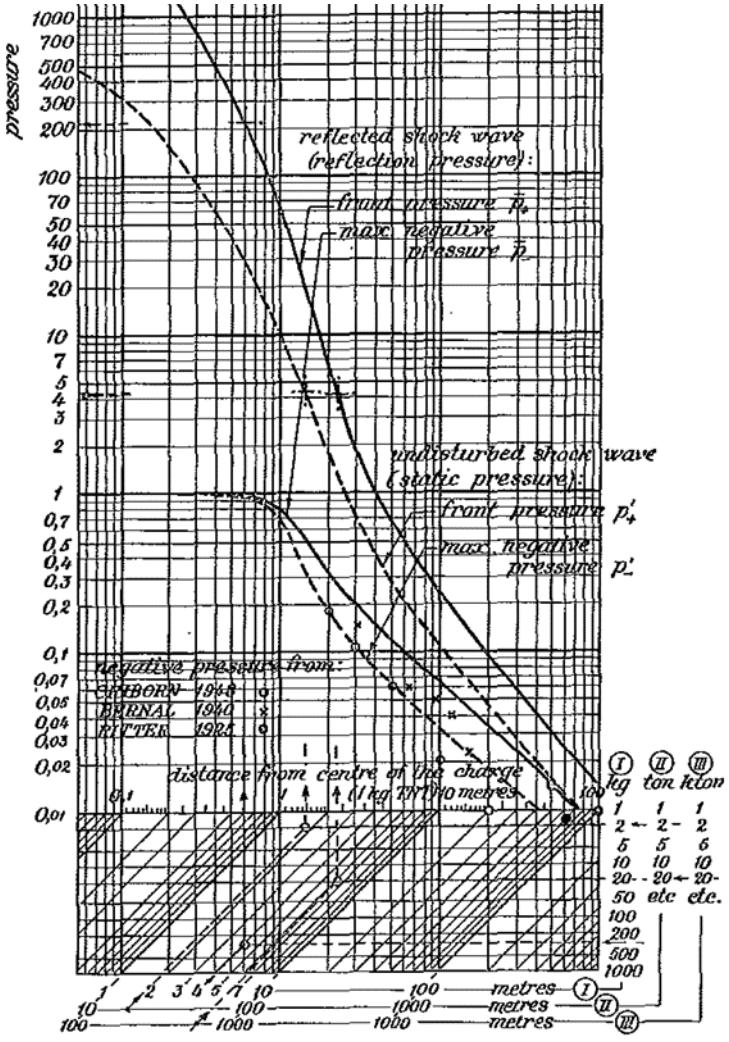

Figure 31: Granström Negative Phase Parameters (Granström 1956)

It is possible that the data presented by Granström (1956) is the same data used to calculate the negative phase blast parameters in the UFC 3-340-02. A definitive origin of the data used to support the parameters presented was not found. It may be possible that the inaccuracy of the blast parameters presented in the UFC 3-340-02 is the source of the difficulty in predicting the negative phase pressure time history. However, sufficient evidence to make a definite conclusion about the accuracy or origin of the UFC 3-340-02 parameters was not ascertained. More research on this topic needs to be conducted before any substantial claims can be made.

Ultimately, no suitable method for predicting the negative phase was obtained. The discrepancies between the observed data and the prediction tools were too great to allow for confident use of a prediction methodology. To create a fully realized fragment prediction methodology a means of accurately predicting the negative phase impulse must be developed. To evaluate the accuracy of the methodology presented in its current form the observed impulse values for each validation test were used for fragment prediction.

Chapter 5: Comparison and Validation

In order to test the validity of the prediction method presented in Chapter 3 test data from two different UNR CMU wall test series were collected. The model was evaluated using two main criteria: wall failure prediction and average fragment velocity. The aim of this validation effort was to determine if the energy balance methodology presented above could be effectively used to predict the fragment velocity of failed CMU walls. Additionally, the ability of the methodology to predict wall failure or non-failure was examined.

5.1 The Engineering Research and Development Center (ERDC) Full-Scale Tests 2019

The ERDC conducted two full-scale tests on UNR CMU walls in the summer of 2019. Reflected pressure and reflected impulse data was collected, as well as wall acceleration and displacement data. The assumption that URN CMU walls fragment into individual blocks was heavily supported by observations made during this testing effort. The first test resulted in wall failure and low fragment velocities; the second test resulted in wall failure and higher fragment velocities. These tests were especially useful for validating the fragment velocity prediction methodology presented in this effort. Twelve pressure gauges and four accelerometers were used to collect pressure time histories and acceleration histories. Two displacement gauges were used to record wall displacements. The acceleration data was integrated to find the wall velocity time histories. Additionally, quality high speed video of both tests was reviewed extensively for velocity information, and also provided a useful validation of the predicted wall failure behavior. The high-speed video facilitated the formulation of the first three assumptions presented in

Section 3.2.1 Assumptions. The high-speed video also provided a useful validation of the predicted wall failure behavior.

The wall used in the first ERDC test can be seen in Figure 32. The pressure gauges and accelerometers can be seen in Figure 33 and Figure 34 respectively.

Figure 32: ERDC Full-Scale Wall Test 1 and 2 with Reaction Structure Pre-Test (ERDC)

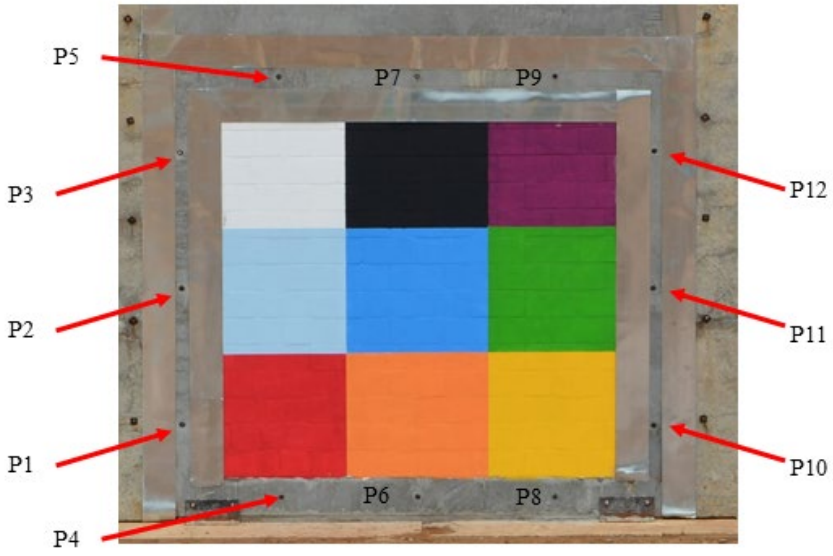

Figure 33: Pressure Gauge Layout Used in ERDC Test 1 and 2 (ERDC)

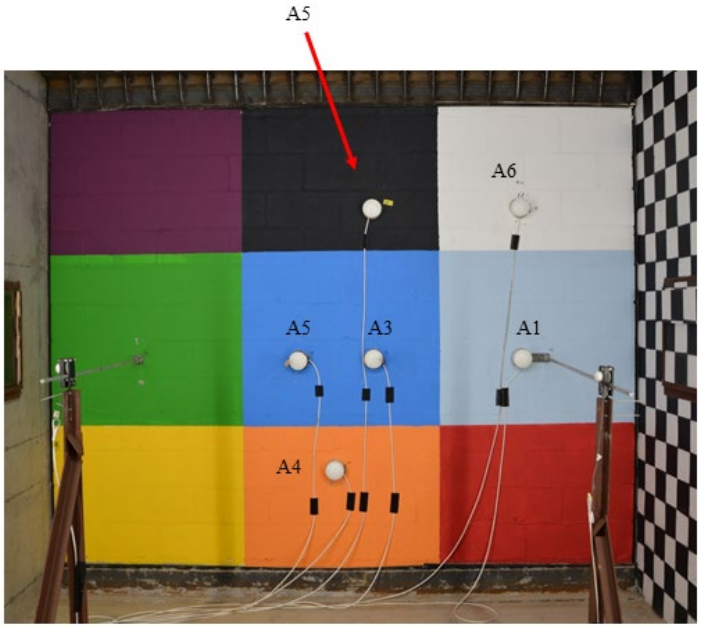

Figure 34: Accelerometer Gauge Layout Used in ERDC Test 1 and 2 (ERDC)

5.2 Quarter-scale Test ERDC 2000 1999 Tests

The ERDC conducted a number of quarter-scale CMU wall tests in 1999 and 2000 for The Technical Support Working Group (TSWG) Office of Special Technology TSWG GAA Administration (2002). A number of 2.9 mm bars (approximately #4 bar) were used as slip dowels in every third grouted cell to attach the top of the wall to the reaction structure. It is unclear how the URN CMU walls were attached to the top of the reaction structure. A gap was left between the sides of the wall and the reaction structure to ensure one-way action. The aim was to provide simple support conditions for the experimental effort, consequently, the finite element modeling efforts following these experiments utilized simple support conditions and one-way action in their analysis. In order to simplify the analysis, and provide consistency between modeling efforts, simple support conditions as well as one-way action were assumed

when modeling the quarter-scale tests during this validation effort. The blocks used in the experiment can be seen in Figure 35, and the test setup can be seen in Figure 36.

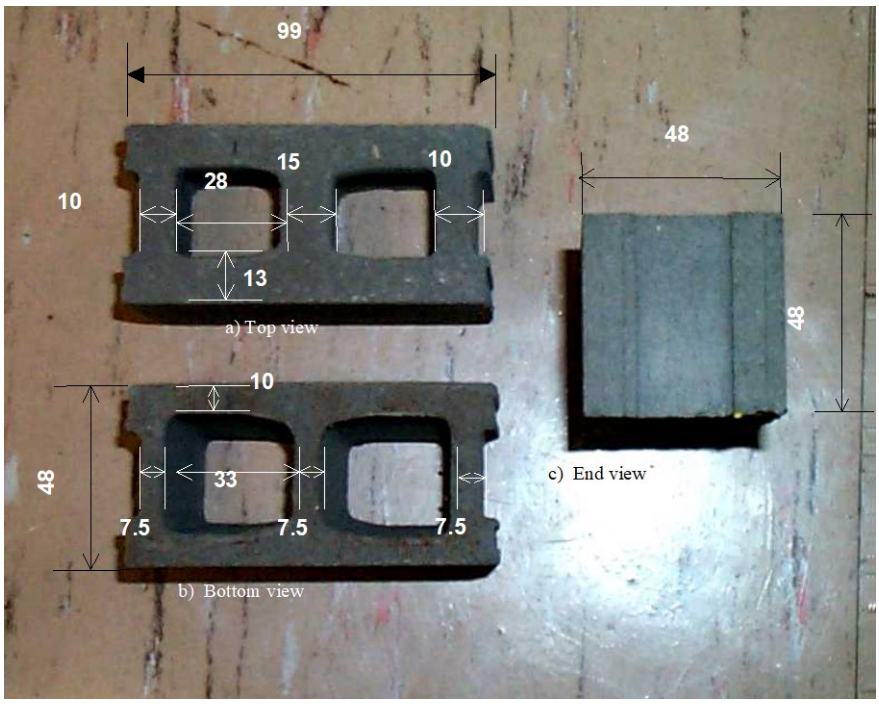

Figure 35: Quarter-scale CMU Dimensions in Millimeters (Baylot et al. 2005)

Figure 36: Quarter-scale CMU Test 1-4 Reaction Structure with Wall (Quarter-Scale Testing 2000)

5.3 Test Data and Predictions

5.3.1 Full-Scale ERDC Test

For ease of analysis, all blocks were assumed to have uniform cross sections; no block tapering along the height of the block was assumed. The geometric and material input values used for velocity prediction are in Table 1. The input values in Table 1 are identical for both tests since they were both conducted with the same CMU blocks and in the same reaction structure. The only difference between the first and second full-scale ERDC tests was the reflected pressure loading.

Table 1: ERDC Full-Scale Test Inputs Test 1 and 2 Used for Fragment Velocity Prediction

Material Properties			
Name	Symbol	Number	Unit
Unit Strength	f'c	2000	psi
Unit Weight	Wu	127.5	pcf
Solid Volume Block	Vb	403.5	in^3
Block Rupture Strength	f_t	200	psi
Mass Block	Mb	29.8	lb
Block and Wall Geometric Properties			
Depth unit (into wall)	t_w	8	in
length unit (along wall width)	ℓ	16	in
Height unit	h	8	in
Void width	t_v	6	in
Void length (total)	ℓ_v	12.9	in
Height wall	L	112	in
Width Wall	B	128	in

Nominal block dimensions were used for calculation since the mortar was not directly accounted for in the model. Utilizing nominal dimensions allowed the wall in the model to have the same number of blocks and overall dimensions as the wall in the test. The model wall also had approximately the same mass as the test wall. The influence of mortar joints on wall size, and mass was accounted for by using nominal block dimensions instead of the actual block dimensions.

The reflected pressure time history for each test was measured by twelve different pressure gauges arrayed around the perimeter of the wall. This data was processed and averaged to create one single reflected pressure time history for each test. To construct a reflected impulse time history, the averaged pressure time history was integrated. For each velocity prediction, a discrete impulse value was selected from the observed impulse curve. This discrete impulse value was utilized, in conjunction with the data from Table 1, to predict a discrete fragment velocity value for the entire wall. Discrete velocity predictions were generated at many different

times during wall failure. These various discrete velocity predictions were plotted against the observed continuous velocity of the wall. The timestamp of each discrete impulse value corresponds to the timestamp of the matching discrete velocity prediction.

To generate a continuous observed wall velocity plot, the accelerometer data was integrated. The accelerometer data was not averaged. Displacement gauge data was used to construct additional velocity time histories. The observed velocity plotted with the predicted velocity at various points in time is presented in Figure 37 and Figure 38. Note that the velocity data has been normalized relative to the maximum observed velocity and the pressure-time history has been normalized to the maximum positive pressure for each full-scale test. The duration has also been normalized to give a maximum value of one.

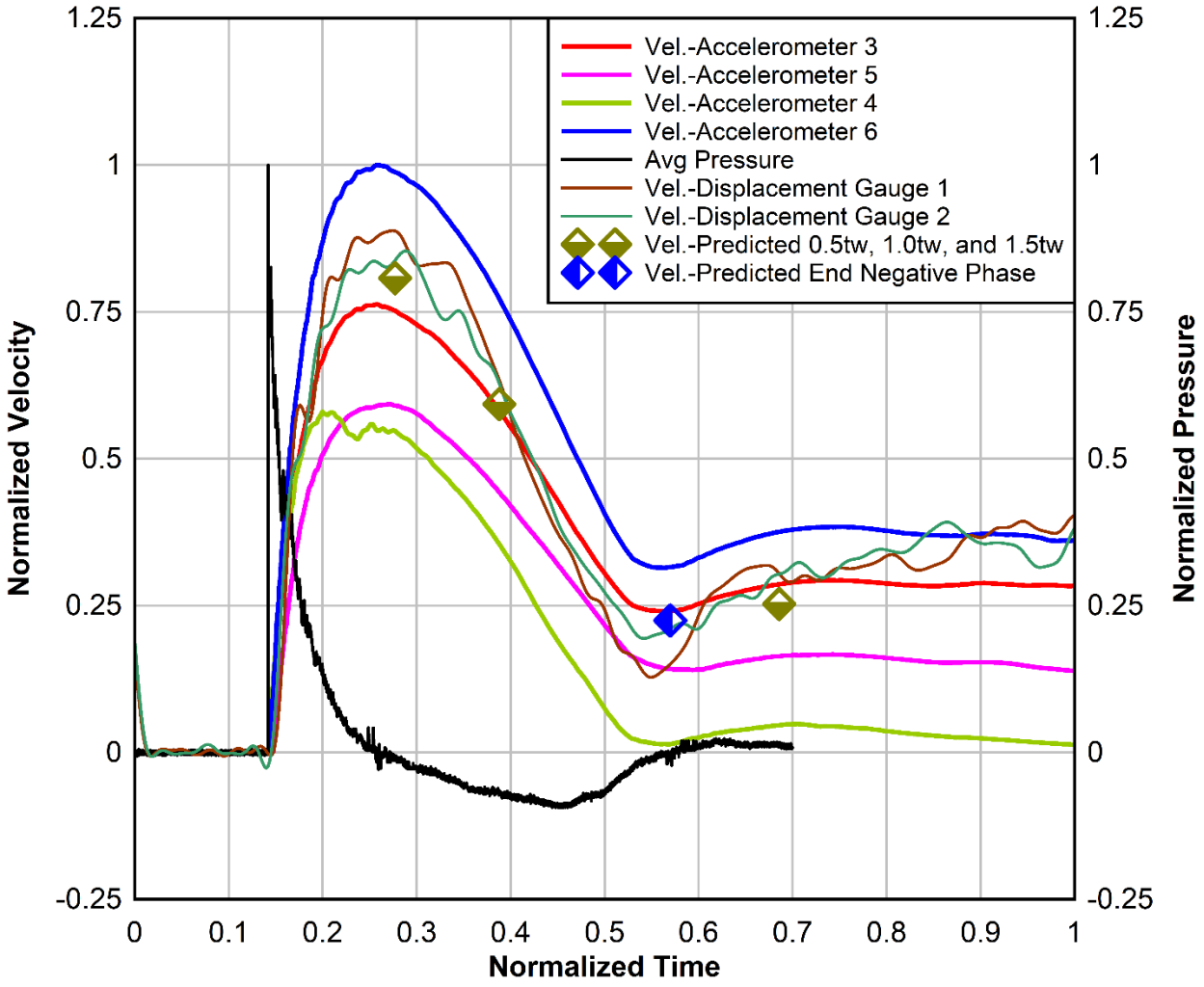

Figure 37: Test 1 Full-Scale ERDC Observed Velocity Data and Predicted Velocity Values

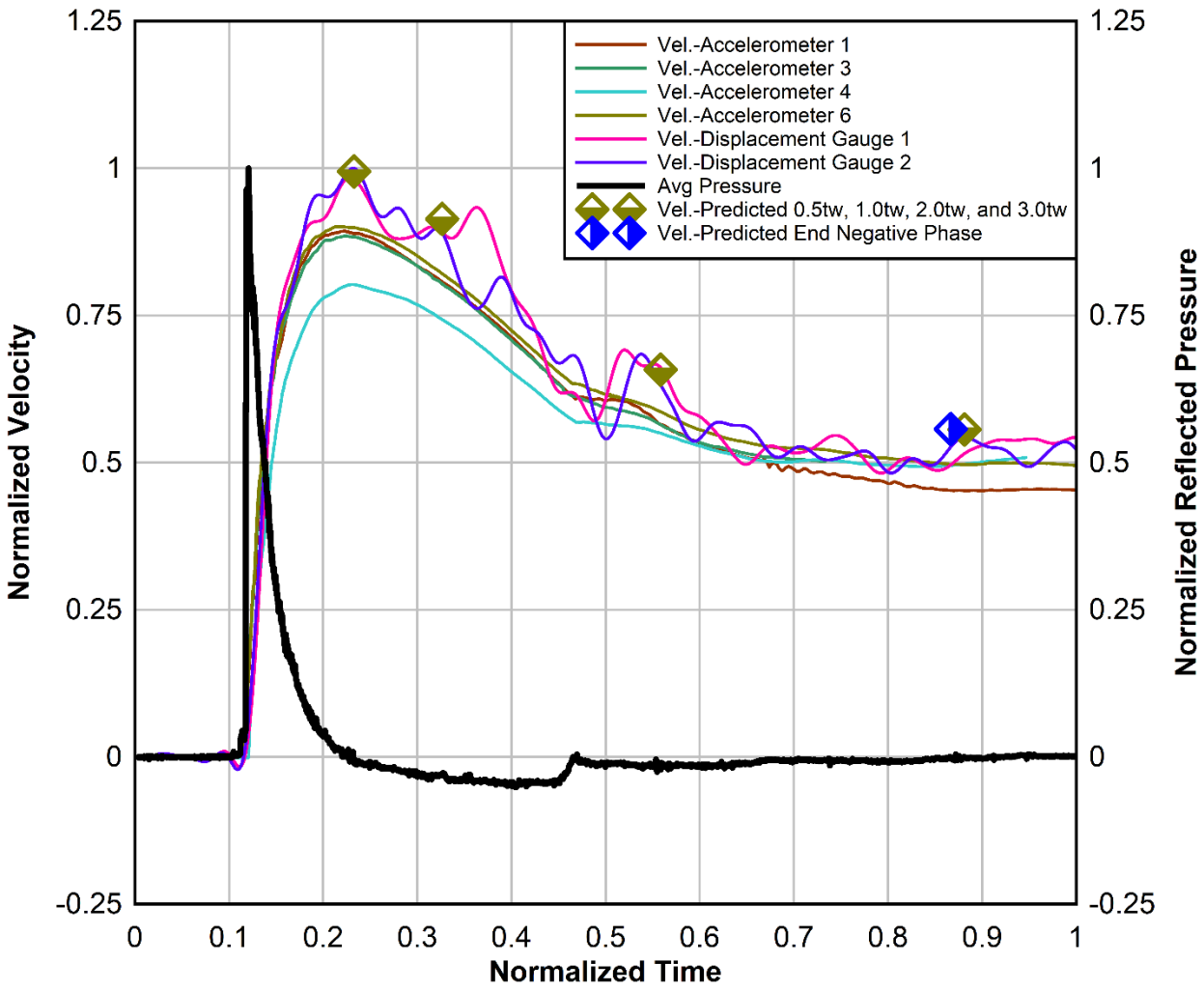

Figure 38: Test 2 Full-Scale ERDC Observed Velocity Data and Predicted Velocity Values

The diamond points on each of the velocity plots are the predicted wall velocities at different points during wall deflection. The points were selected to correspond to different wall displacements and the end of the negative phase loading. The average reflected pressure on the wall was also displayed to illustrate the variability of the negative phase loading. The reflected pressure is an average of the various pressure gauges for each test. Accelerometer data was integrated to give velocity plots. Additionally, displacement gauges were used to construct extra velocity time histories for these full-scale tests.

For the first test, no data manipulation was conducted on the reflected pressure. Each of the pressure gauges was averaged over time to yield a total average pressure value. For full-scale test 2 some pressure gauge data was discarded before averaging. Pressure gauge five, eight, and ten were all removed before averaging occurred. The pressure data from these gauges was erratic and did not match what was expected and what the other pressure gauges recorded, so they were discarded. Additionally, for full-scale test 2 the time of arrival for each pressure gauge was shifted to the average time of arrival for the remaining pressure gauges. Originally each pressure gauge recorded a slightly different time of arrival for the pressure wave incident on the wall. Since all the reflected pressure gauges were the same distance from the origin of the blast wave this was unexpected. Ultimately, it was decided that this discrepancy was due to a problem with the data recording method, since all the pressure readings looked correct, they were simply shifted in time relative to each other. To correct this issue without introducing more errors, the pressure data for each gauge was simply shifted in time. The arrival time is when the pressure reading spikes significantly to indicate the arrival of the reflected pressure wave. The arrival time was then averaged between each of the pressure gauges, and all the pressure time histories were shifted to have an arrival time of this average value. After this manipulation was conducted, the average of each pressure gauge was taken to construct the average reflected pressure time history for test 2.

There were four accelerometers used in full-scale test 1, and six used in full-scale test 2. However, two of the accelerometers failed during full scale test 2. The data from both of these accelerometers was discarded and is not shown in the figures.

5.3.2 Quarter-scale TSWG Test

The quarter-scale tests were analyzed in the same manner as the ERDC tests. The input data used for velocity prediction is presented in Table 2. Four different quarter-scale tests were examined from the TSWG effort. Each test had identical material and geometric properties, the only variation between tests was the input loading.

Table 2: TSWG Quarter-Scale Test 1-4 Material and Geometric Input Data Used for Fragment Velocity Prediction

Material Properties			
	Symbol	Number	Unit
Unit Strength	f'c	2000	psi
Unit Weight	Wu	109.4	pcf
Solid Volume Block	Vb	9.3	in^3
Block Rupture Strength	f_t	200	psi
Mass Block	Mb	0.59	lb
Block and Wall Geometric Properties			
Depth unit (into wall)	t_w	1.9	in
length unit (along wall width)	ℓ	4	in
Height unit	h	2	in
Void width	t_v	0.98	in
Void length (total)	ℓ_v	2.9	in
Height wall	L	32	in
Width Wall	B	64	in

The block dimensions reported here were increased to account for the lack of mortar in the model. The block dimensions were increased to create a wall with the same number of blocks and overall wall dimensions as the one used in the testing effort. The mass and size of mortar joints were accounted for by increasing overall block size. Additionally, the model did not account for the tapering of the block walls. An average value was taken for the block dimensions to give blocks with vertical sides of approximately the same mass as the blocks with tapered

sides used in the quarter-scale test. Ultimately, the block dimensions used in the modeling effort should serve as an adequate representation of the blocks used in the testing effort. More detailed calculation of block dimensions was not undertaken due to the limited available data regarding the actual blocks used. Block dimensions and masses should be taken as approximate but accurate within the overall accuracy of the engineering level model presented.

Four pressure gauges were mounted around the perimeter of the quarter-scale CMU wall to measure the reflected pressures experienced by the wall. These pressures were averaged and integrated to create an average pressure time history and impulse curve. The observed impulse curve was used to create the input energy for the velocity prediction operations.

Two accelerometers were mounted on the inside of each wall, one at midspan and the other at 1/4 span (Dennis et al. 2002). The accelerometer data was integrated to generate two velocity time histories for each test. Several discrete impulse values were selected from the pressure time history and utilized to predict discrete wall velocities at various points in time. The velocity prediction values are plotted blow in Figure 39, 40, 41, and 42 with the continuous observed velocity data. Note that the velocity data has been normalized relative to the maximum observed velocity, and the pressure time history has been normalized to the maximum positive pressure for each quarter-scale test. The duration has also been normalized to give a maximum value of one. The first accelerometer in the test 3 detached from the wall and entered free flight at the peak positive pressure.

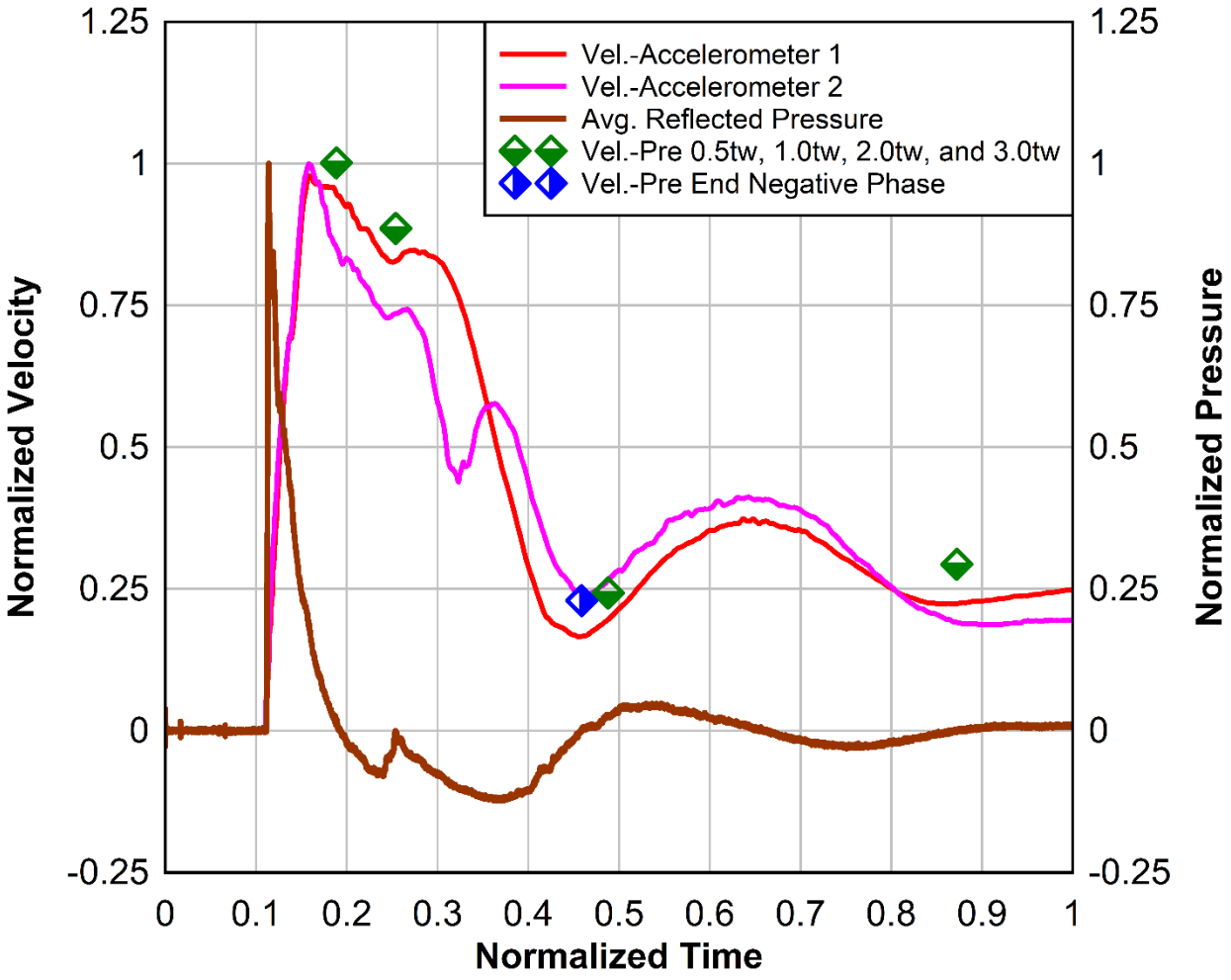

Figure 39: Test 1 Quarter-scale Velocity Data with Predictions

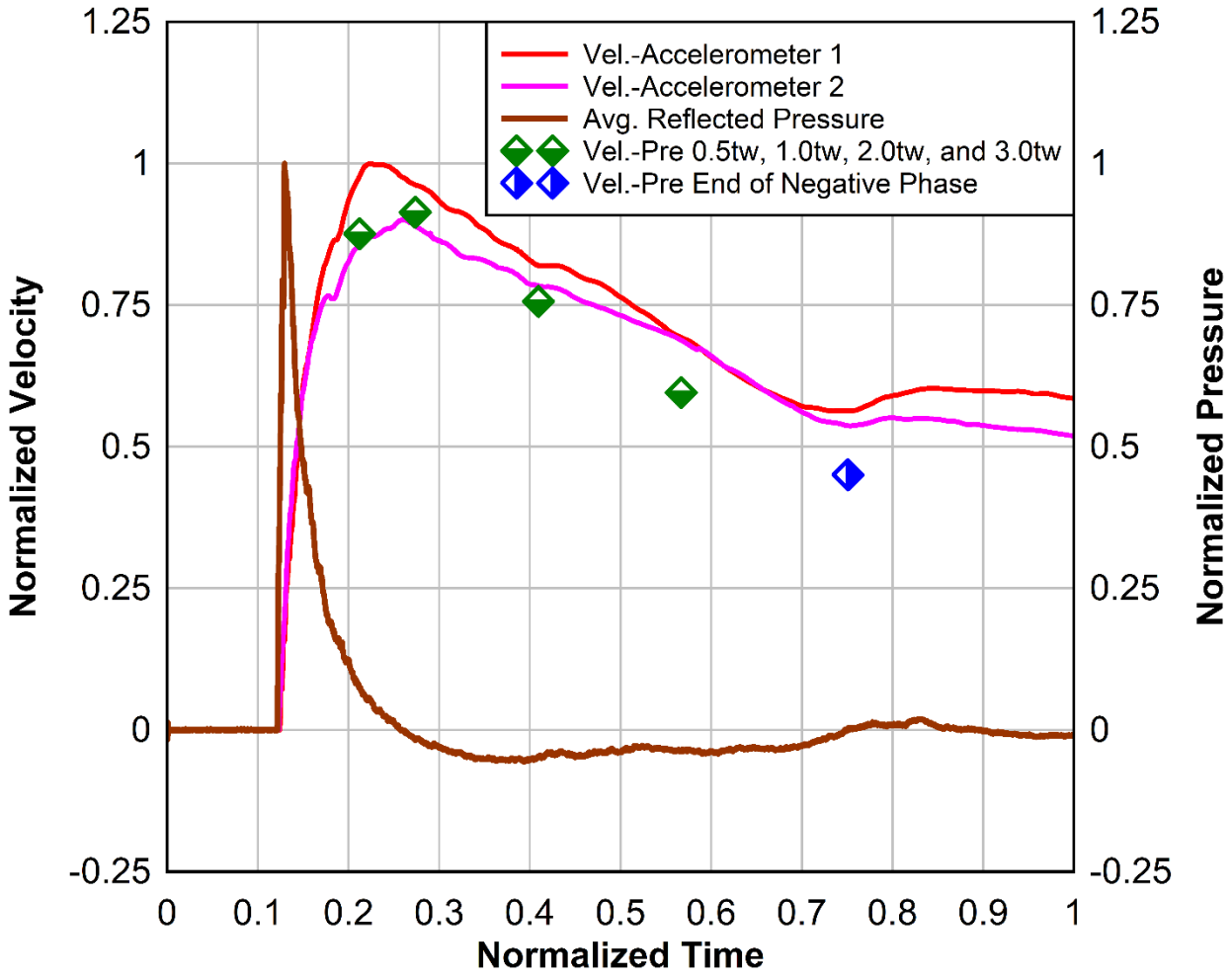

Figure 40: Test 2 Quarter-Scale Velocity Data with Prediction

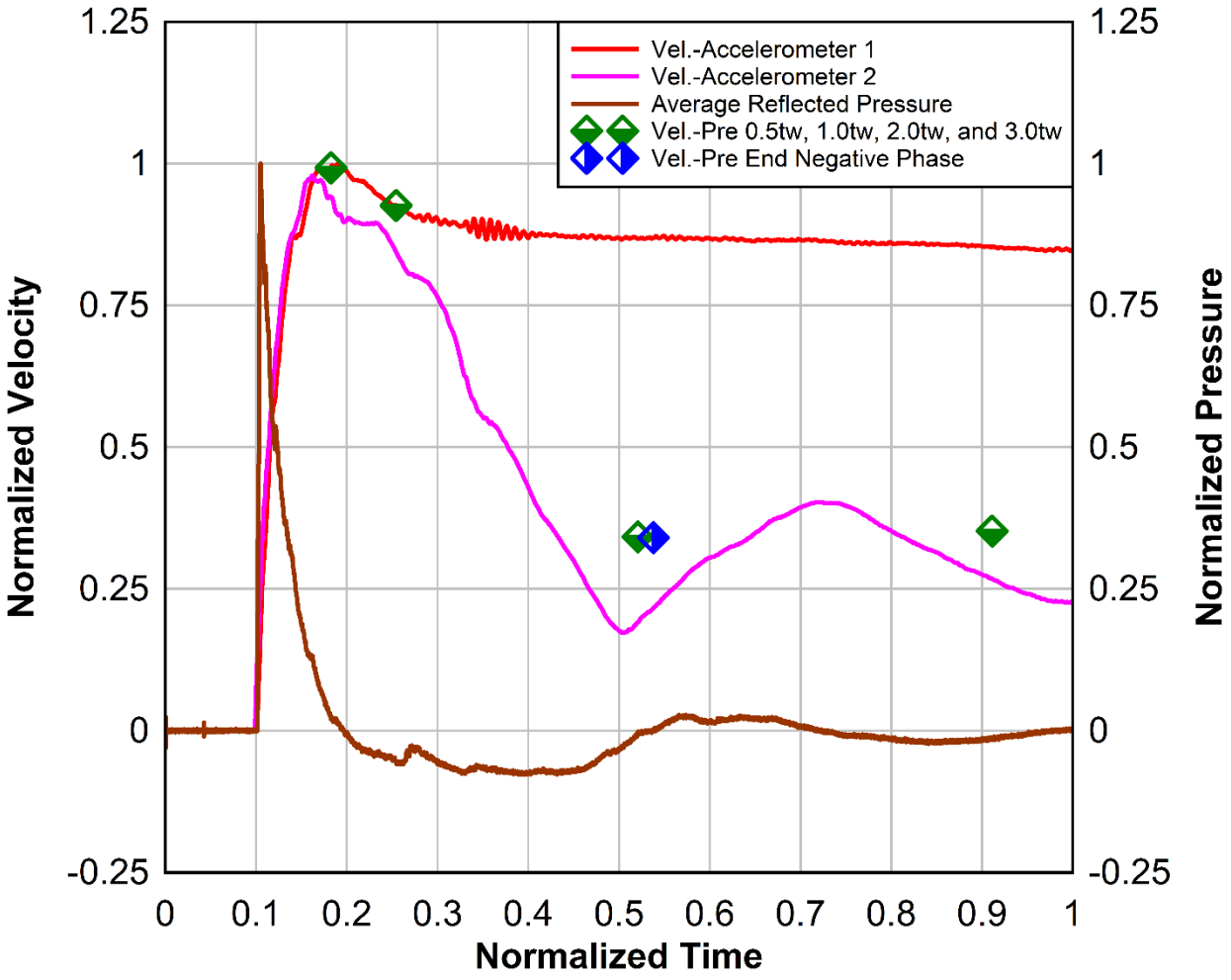

Figure 41: Test 3 Quarter-Scale Velocity Data with Prediction

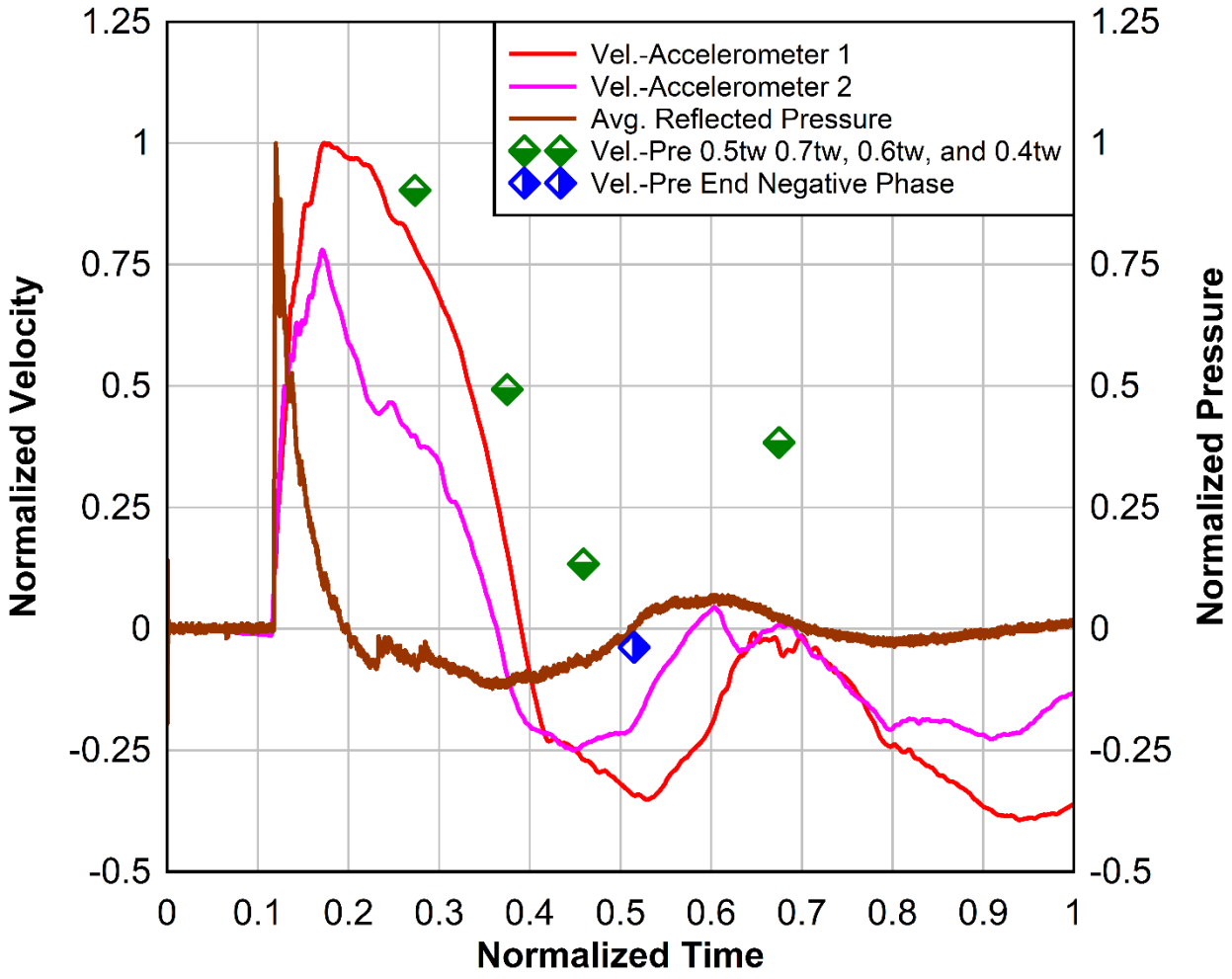

Figure 42: Test 4 Quarter-Scale Velocity Data with Prediction

The diamond points on each of the velocity plots are the predicted wall velocities at different points during wall deflection. The points were selected to correspond to different wall displacements and the end of the negative phase loading. The average reflected pressure on the wall was also displayed to illustrate the variability of the negative phase loading. The reflected pressure is an average of the various pressure gauges for each test. Accelerometer data was integrated to give velocity plots.

5.4 Discussion

In order to better understand the behavior of the walls as they deformed and the nature of the velocity being predicted, multiple wall velocity predictions were conducted for each test. The discrete free flight velocity was predicted for each full-scale and quarter-scale test. The discrete velocity prediction utilized the observed discrete impulse value at the end of the negative phase to calculate the input energy. The predicted velocity value was assumed to be the average fragment velocity when the blast load was no longer acting on the fragments. At this point in time the fragments were in free flight. They were still being acted on by gravity and air resistance, but most energy from the blast wave had already been imparted to the fragments. This value should be utilized to make any predictions about the flight of fragments. Additionally, several velocity predictions were made for each test based on the wall displacement. This provided insight into the possible relationship between wall displacement and free flight velocity.

The quarter-scale data show some interesting trends between the observed experimental data and the predicted velocities, since these tests cover a wider range of explosive input energies. The energy absorption term in the energy balance is significantly less than the input energy for every test except quarter-scale test 4. Ultimately, the brittle nature of the wall resulted in very little potential for energy absorption. Parameters associated with the wall material and geometric properties, like bond strength, wall dimensions, and block sizes have little influence on the fragment velocity at large input energies because the strain energy developed is so small compared to the input energy. The input energy from the blast wave has a significant influence on the final fragment velocity for all walls. This was expected since the energy imparted to a system from an explosive loading event is usually quite large when compared to the energy

absorption potential of an UNR CMU wall. Ultimately, reducing the input energy term inside the energy balance will help reduce the fragment velocity the most. Similarly, fragment velocity can also be reduced by increasing the mass of the wall.

Generally, the predicted velocity was larger than the experimentally observed velocity. This phenomenon was observed in all the tests except the second quarter-scale test. Of all four quarter-scale tests, the second was the most violent and produced the highest peak pressures and impulses. It may be possible that the input energy formulation breaks down at higher energies, or that the high pressures associated with the second quarter-scale test caused irregularities in the experimental data collection. The adopted resistance function may also breakdown at higher reflected pressures. The second test behaved quite differently compared to any other test examined. Ultimately, it is unclear what caused these anomalies, it may be related to the increased input energies, however, only six total data sets were examined so it is difficult to draw conclusions from one test.

It was originally hypothesized that the fragments would enter free flight at about one wall thickness of deflection since this is when the wall no longer provides any resistance. However, it was observed that at one wall thickness deflection, the negative pressure produced by the blast wave was still reducing the fragment velocities. The value calculated for strain energy absorption was not reduced for the half wall thickness deflection velocity prediction. This is ultimately incorrect since according to the adopted resistance function the full strain energy of the wall is not developed until the wall displaces one wall thickness. The wall velocity prediction before one wall thickness is not the overall goal of the current effort, and the strain energy has little effect on the velocity prediction for most of the tests, so this slight discrepancy was deemed acceptable.

The following trends were observed between wall velocity and wall deflection. It should be noted that all wall deflections are calculated at the height of the accelerometer, which was generally at or around mid-height of the wall. Peak velocity generally occurred around one-half of a wall thickness deflection. Interestingly, the end of the negative phase loading generally corresponded to the point when wall deflection was two to three times the wall thickness. After the wall had deflected two total wall thicknesses, its velocity was relatively stable. By the time three wall thicknesses of deflection had occurred, wall velocity was generally even more stable. This indicates that all major loading on the wall was completed. The first full-scale test and the fourth quarter-scale test deviated from the deflection behavior of the other walls. The first full-scale test was a "slow" wall failure; the overall shape of the wall velocity response was typical. The velocity sharply increased and then more slowly decreased to eventually level off. The maximum wall deflection was about one and a half wall thicknesses. This was likely due to the lower input energy.

Since there is currently no effective way to predict the end of the negative phase loading, it may be possible to utilize the deflection value of two to three wall thicknesses as an alternative. If one could iteratively step through wall deflections and calculate fragment velocities, it might be possible to use the deflection criteria as a free flight condition since both the end of the negative phase and two to three wall thicknesses of deflection seem to correspond to about the same point in time. It should be noted that the second quarter-scale test does not exhibit this behavior, since its velocity never really stabilizes.

Quarter-scale test 4 predicts a negative velocity at the end of the negative phase. Negative predicted velocities simply indicate that the fragment is traveling towards the explosive. The accelerometers also reported negative velocities at the end of the negative phase. The wall in the

quarter-scale test 4 moved inward and outward but did not fail and produce fragments (Baylot et al. 2005). For UNR CMU walls this is a very narrow range of input energies, but it is not negligible. It should be noted that quarter-scale test 4 was the slowest of the quarter-scale tests and did not displace past 0.7 times the wall thickness.

The wall behavior exhibited by quarter-scale test 4 supports the conclusion reached in Section 3.6 Utilizing Energy Formulation for Wall Failure Criteria that input energies less than the strain energy absorption potential of the wall result in wall non-failure. Here "non-failure" is limited to negligible positive fragment velocities. It is possible that the wall may still be standing in the "non-failure" state; however, it is also possible that the wall may still collapse and simply not generate fragments with significant positive velocities. Here "significant positive velocity" is taken to mean a fragment velocity that is high enough to cause harm to an individual behind the wall. The fourth quarter-scale test is the only validation test that supports the failure prediction aspect of this effort. The wall was predicted to be in a non-failure state, and this was seen in the experiment. This test only provides one data point to examine the failure/non-failure prediction component of this methodology. The accuracy of the other tests should help support the overall accuracy of the methodology. This methodology has limitations and is quite simple; therefore, caution is urged when using this methodology to evaluate failure of a CMU wall. The approximate engineering level nature of the presented methodology prevents a more accurate prediction of non-failure wall behavior.

Full-scale test 1 created fragments with considerably lower velocities compared to the second full scale test. As a result of this, the wall only deflected about one wall thickness before its velocity stabilized. The velocities observed in this test were considerably more variable between accelerometers when compared to the second test. No viable theory has been devised on

the cause of this variability. However, the discrete predicted velocities do fall inside the range of velocities reported during testing. This indicates that the prediction method is relatively accurate. Finally, all of the observed velocities for the first full-scale test stabilize after the end of the negative phase.

The second full-scale test exhibits all of the same behaviors seen in the quarter-scale tests. The velocity stabilizes around two wall thicknesses of deflection and peaks around one-half wall thickness deflection. Three wall thicknesses of defection roughly corresponds to the end of the negative phase. Overall, the predicted velocities are fairly close to the observed velocities for full-scale test 2. The assertion that the end of the negative phase corresponds to the end of wall loading is supported by both the quarter-scale and full-scale tests.

Since the proposed method of predicting fragment velocities provided reasonably accurate velocity predictions for a total of six different tests over many different input energy ranges and two different wall geometries, the energy method developed is a recommended fast-running method to predict fragment velocities for the failure of an UNR CMU wall, but there are a number of limitations to this method. The proposed methodology should be utilized for estimation, field velocity prediction, and preliminary velocity measurements only. For design use, more accurate and reliable methods should be employed.

Chapter 6: Analysis Example

6.1 Analysis Scenario

In order to provide a better understanding of how to apply the proposed methodology, an analysis example has been created. It will be shown how to predict the fragment velocity of the first test from the quarter-scale TSWG data. This should aid in implementing the proposed methodology correctly, and aid in answering any logistical questions not directly addressed in the explanation above.

6.2 Input Determination

Geometric, material, and loading information are required to conduct a velocity prediction. The geometric and material inputs required are presented in Table 3. It should be noted that f'_c is the compressive strength of the block only. The compressive strength of the block mortar system (f'_m) is not required. The block strength is only used to estimate the modules of elasticity and not for strength calculations. The nominal unit dimensions should be used for input. Mortar thickness is not included in any of the strength or geometric formulations, so the model effectively uses the mass of a wall completely full of concrete masonry units with no mortar. The mortar strength is accounted for in the tension strength value selection.

Table 3: Analysis Example Geometric and Material Inputs

Material Properties				
	Symbol	Number	Unit	Description
Unit Strength	f'_c	2000	psi	Compressive strength of block
Unit Weight	Wu	109.4	pcf	Unit weight of block material
Block Rupture Strength	ft	200	psi	The limiting tensile strength of the wall (block strength or mortar block interface strength)
Block and Wall Geometric Properties				
Depth unit (into wall)	t_w	1.9	in	Thickness of wall
Length unit (along wall width)	ℓ	4	in	Length of each unit, along the width of the wall
Height unit	h	2	in	Unit height
Void width	t_v	0.98	in	The void width, void is assumed to be uniform along unit height
Void length (total)	ℓ_v	2.9	in	Total void length along width of wall (both holes)
Height wall	L	32	in	Total height of wall
Width Wall	B	64	in	Total width of wall

After the geometric and material inputs are collected, loading information must be collected. The specific impulse value at the end of the negative phase is required. Currently there is no viable method to predict this impulse so an observed pressure time history must be used to generate the required impulse curve. Figure 43 shows the reflected pressure time history and corresponding impulse curve from the first TSWG test.

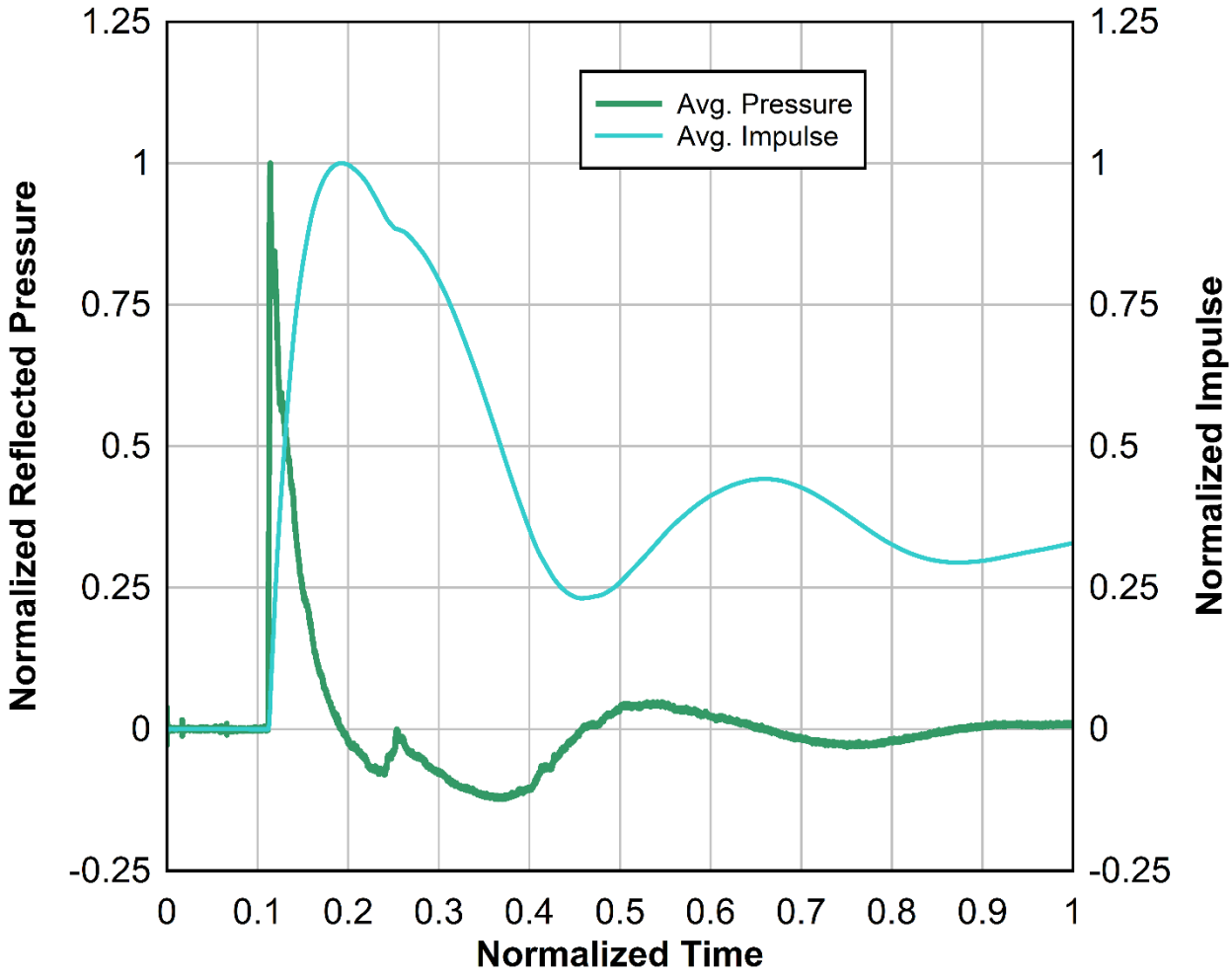

Figure 43: Pressure-Time History of TSWG Test 1

A discrete impulse value must be selected that corresponds to the end of the negative phase. For the current example the end of the negative phase occurs at roughly 0.46 time. The impulse value is recorded at that time and then utilized for input energy calculations. To utilize Equation (3.9) the specific impulse must be calculated as well as the wall mass. Table 4 shows the impulse value extracted from Figure 43 and the converted specific impulse value required for Equation (3.9). The recorded impulse value is multiplied by the effective area of the wall to generate the specific impulse required for energy calculations. This effective wall area is the area

of the wall minus the area of the top and bottom rows of block. See the end of Section 3.4.2 Input Energy for a defense of the use of an effective wall area.

Table 4: Input Energy Calculation

	Value	Unit
Normalized Time	0.46	-
Normalized Impulse - recorded	0.23	-
Normalized Specific Impulse	0.41	-

6.3 Computation

After input collection and manipulation, the equations presented in Section 3.4 Energy Balance Theory are utilized to calculate the resistance of the CMU wall and produce a discrete velocity prediction. First, Equation (3.12) is utilized to calculate the moment of inertia of a single block, the moment of inertia can also be found in standard tables. Then Equations (3.2) and (3.3) are used to calculate the elastic resistance and elastic displacement of the wall. For UNR CMU walls this value is extremely small compared to the thickness of the wall. After collecting these terms, Equation (3.20) is used to calculate the strain energy associated with the elastic deflection of the CMU wall.

Table 5 shows the values generated for each of the elastic resistance terms. It should be noted that the maximum resistance and elastic displacement are calculated for a unit beam one block wide and the elastic strain energy is calculated for the entire wall.

Table 5: Elastic Resistance Terms

	Symbol	Value	Unit
Max Resistance elastic	Q_1	106.7	lb.
Elastic Displacement	Y_1	0.0134	in.
Strain Energy Elastic	Estrain1	7.30	lb-in.

After the elastic terms are generated the secondary resistance parameters must be obtained. Equation (3.4) is utilized to calculate the secondary resistance. For an UNR CMU wall this value will always be significantly lower than the elastic resistance. Significant axial force is the only way to drastically increase the secondary resistance. This changes the overall response mechanism for the wall. The wall configuration that this methodology has been developed for results in a secondary resistance that will always be significantly lower than the elastic resistance. However, due to the even more pronounced difference between the elastic and secondary resistance displacements the energy absorbed by the secondary resistance mechanism is significantly larger than the elastic mechanism. Equation (3.26) is utilized to calculate the secondary strain energy. Table 6 shows the secondary resistance and the secondary strain energy for the current wall. Similar to the elastic terms, the secondary resistance is for a unit beam one block wide and the strain energy is for the entire wall.

Table 6: Secondary Resistance Terms

	Symbol	Value	Unit
Max Secondary Resistance	Q_2	2.22	lb
Total Strain Energy of Secondary Res	Estrain2	33.3	lb-in

Both the elastic and secondary strain energy terms are combined using Equation (3.27). The kinetic energy input into the wall is generated by Equation (3.9). Finally, Equation (3.28) is

utilized to calculate the total kinetic energy of the system. Table 7 shows the total combined strain energy terms and the energy input into the system from the explosive.

Table 7: Total Energy Terms

	Symbol	Value	Unit
Energy Absorbed	E	40.6	lb-in
Energy Input Total	Eng in	994	lb-in
Energy Input Total	Eng in	82.8	lb-ft

Finally, the input energy and absorbed strain energy are utilized in Equation (3.29) and (3.31) to calculate the predicted wall velocity. Table 8 shows the total kinetic energy of the wall and the normalized velocity of each individual block.

Table 8: Kinetic Energy and Velocity Terms

	Symbol	Value	Unit
Total Kinetic Energy	KEt	953	lb-in
Normalized Velocity of Block	V	0.02	-

6.4 Outputs of Analysis

By utilizing the procedure demonstrated above it is possible to predict the velocity of a CMU wall fragment given the wall geometry and material parameters as well as the observed pressure time history acting on the wall. If the above procedure is repeated for multiple input energy values (by using different discrete impulse values at different points in time for the same loading event) and those velocity predictions are plotted, Figure 44 can be produced.

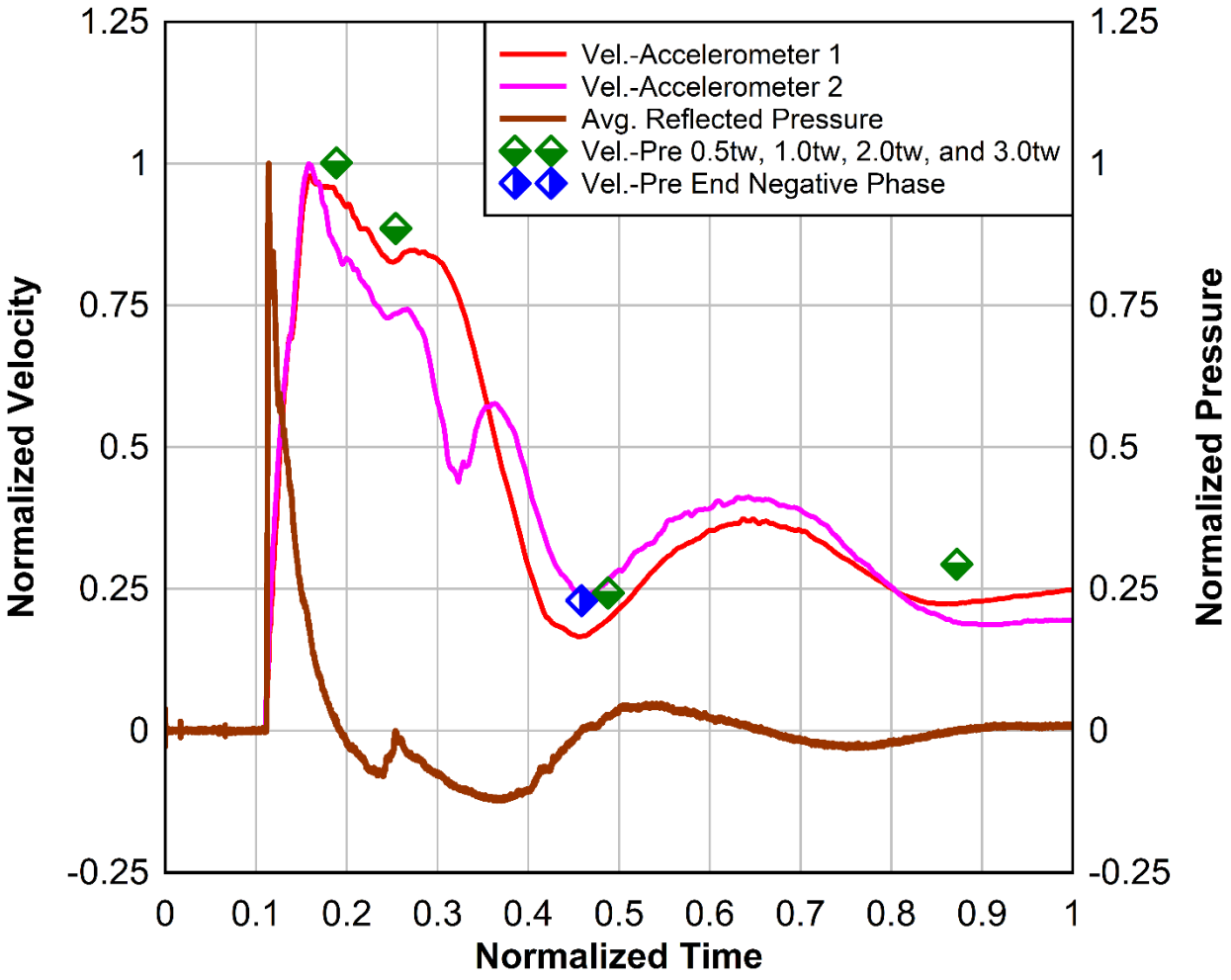

Figure 44: Example Output of Velocity Prediction Methodology

Chapter 7: Conclusion

An energy balance methodology has been developed to predict the dynamic blast failure of an UNR CMU wall and to calculate the free flight velocity of wall fragments produced by that dynamic failure. An energy balance which accounts for the energy imparted to the wall by a blast wave, the energy absorbed by the wall as it deflected, and the energy imparted to wall fragments after failure was developed. Assumptions about the behavior of the wall during loading and breakup were discussed and defended. A resistance function was adopted to aid in the calculation of the energy absorbed by the wall during deflection and failure. The input energy was selected to include the pronounced impact of the negative phase pressure on wall fragment velocity. A negative phase pressure history prediction methodology was examined but ultimately abandoned, because of differences between the available prediction methodologies and the data examined. No acceptable method was discovered in the available literature. Possible reasons for the discrepancy between the observed negative pressure phase behavior and the predicted behavior were stated and briefly examined. A simple kinetic energy formulation was used to calculate the velocity of each of the individual wall fragments. The methodology was compared to six different CMU wall fragmentation tests. Finally, a simple analysis example was used as an illustration and to aid in the understanding of the operation of this energy balance methodology.

Ultimately, the above methodology should provide a mechanically sound and reasonably accurate method to predict fragment velocities of CMU walls. This should aid in the development of more rigorous and accurate fragment velocity predictions methods. The

methodology should also prove helpful in situations where quick and accurate fragment velocity predictions are desired. The proposed energy methodology should produce reliable and fairly accurate fragment velocity predictions and aid in wall failure prediction.

Recommended future work includes: formulating an effective method for negative phase pressure prediction that can be utilized in a fast-running capacity, and expanding the fragment velocity prediction capabilities of this methodology to include; grouted and unreinforced CMU walls, grouted and reinforced CMU walls, CMU walls with different support conditions, reinforced concrete walls, and other wall material types with fragmentation potentials. Negative phase prediction is separate from the fragment prediction methodology, but it is integral to the accurate prediction potential of this model. Additionally, a more comprehensive negative phase prediction methodology is essential to flexible and impulsive structural response. The overall energy balance methodology should hold for different wall types. By adjusting the assumptions and mechanics for each particular wall type, it should be possible to give reasonably accurate fragment velocity predictions for other types of CMU walls.

References

*Bernal, J. D. (1940). The Physics of Air Raids. *Proc. Roy. Inst. Gr. Brit., XXXI*(1939-49), 262-279.

*Criborn, C. O. (1948). *Shock Waves in Air Recorded by Corona Microphones*. Retrieved from Sweden:

*Ritter, F. (1925). Messungen bei Explosionen mit Nutzanwendung auf den Bergbau. *Zs. Ver. deutsch. Ing, 69*, 1527-1530.

Ahmad, H. (2018). *Masonry Structures: Behavior and Design, 4th Edition*. Longmount Colorado The Masonry Society.

American Concrete Institute. (2014). Building Code Requirements for Structural Concrete. In. Farmington Hills MI: American Concrete Institute.

Baylot, J. T., Bullock, B. M., Slawson, T. R., and Woodson, S. C. (2005). Blast Response of Lightly Attached Concrete Masonry Unit Walls. *Journal of Structural Engineering*, 1189-1193.

Bewick(a), B., Rolater, G., Bui, J., Barsotti, M., Ziemba, A., Sanai, M., and Laney, C. (2017). *Fragmentation of Solid Materials Using Shock Tubes. Part 1: First Test Series in a Small-Diameter Shock Tube* (DTRA-TR-17-21). Retrieved from Defense Technical Information Center: https://apps.dtic.mil/dtic/tr/fulltext/u2/1025099.pdf

Bewick(b), B., Rolater, G., Bui, J., Barsotti, M., Ziemba, A., Sanai, M., and Laney, C. (2017). *Fragmentation of Solid Materials Using Shock Tubes. Part 2: First Test Series in a Large-Diameter Shock Tube*. Retrieved from Defense Technical Information Center: https://apps.dtic.mil/dtic/tr/fulltext/u2/1043784.pdf

Bewick(c), B., Rolater, G., Bui, J., Barsotti, M., Ziemba, A., Sanai, M., and Laney, C. (2018). *Fragmentation of Solid Materials Using Shock Tubes. Part 3: Second Test Series in a Small Diameter Shock Tube.* Retrieved from Defense Technical Information Center: https://apps.dtic.mil/dtic/tr/fulltext/u2/1061869.pdf

Biggs, J. M. (1964). *Introduction to Structural Dyamics*. New York: McGraw-Hill Book Company.

Clayton, J. D. (2008). A Model for Deformation and Fragmentation in Crushable Brittle Solids. *International Journal of Impact Engineering*, 269-289.

Davidson, J. S., Fisher, J. W., Hammons, M. I., Porter, J. R., and Dinan, R. J. (2005). Failure Mechanisms Of Polymer-Reinforced Concrete Masonry Walls Subjected to Blast. *Journal of Structral Engineering ASCE*, 1194-1205.

Dennis, S. T., Baylot, J. T., and Woodson, S. C. (2002). Response of 1/4-Scale Concrete Masonry Unit (CMU) Walls to Blast. *Journal of Engineering Mechanics*, 134-142.

Department of Defense. (2008). *Structures to Resist the Effects of Accidental Explosions* (UFC 3-340-02). Retrieved from https://www.wbdg.org/FFC/DOD/UFC/ARCHIVES/ufc_3_340_02.pdf

Dharani, L. R., and Wei, J. (2004). Dynamic Response of Laminated Glass Under Blast Loading Effect of Negative Phase. *Structures Under Shock and Impact VIII*, 181-190.

Dinan, R., Fisher, J., Hammons, M. I., and Porter, J. R. (2003). *Failure Mechanisms in Unreinforced Concrete Masonry Walls Retrofitted With Polymer Coatings*. Retrieved from Defense Technical Information Center: https://apps.dtic.mil/dtic/tr/fulltext/u2/a587280.pdf

Eamon, C. D., Baylot, J. T., and O'Daniel, J. L. (2004). Modeling Concrete Masonry Walls Subjected to Explosive Loads *Journal of Engineering Mechanics*, 1098-1106.

Englman, R., Rivier, N., and Jaeger, Z. (1988). Size-Distribution in Sudden Breakage by the use of Entropy Maximiation. *Journal of Applied Physics*, 4766-4768.

Friedlander, F. G. (1940). The Diffraction of sound pulses I. Diffraction by a semi-infinite plane.

Gagnet, E. (2013). *Static Resistance Functions for Unbounded Retrofit Unreinforced Concrete Masonry Walls with Plate Connection for Blast Design Applications.* (Masters of Science). Auburn University, Auburn.

Glenn(a), L. A., and Chudnovsky, A. (1986). Strain-Energy Effects on Dynamic Fragmentation. *Journal of Applied Physics*, 1379-1380.

Glenn(b), L. A., Gommerstadt, B. Y., and Chudnovsky, A. (1986). A Fracture Mechanics Model of Fragmentation. *Journal of Applied Physics*, 1224-1226.

Gommerstadt, B. Y., and Chudnovsky, A. (2005). Modeling of Dynamic Fragmentation in Brittle Solids. *Strength, Fracture and Complexity*, 117-126.

Grady, D. E. (1982). Local Inertial Effects in Dynamic Fragmentation. *Journal of Applied Physics*, 322-325.

Grady, D. E. (1988). The Spall Strenght of Condensed Matter. *J. Mech. Phys. Solids, 36*(3), 353-384.

Grady, D. E. (1990). Particle Size Statistics in Dynamic Fragmentation. *Journal of Applied Physics*, 6099-6105.

Grady, D. E., and Kipp, M. E. (1980). Continuum Modelling of Explosive Fracture in Oil Shale. *Int. J. Rock Mech. Min. Sci. & Geomech. Abstr, 17*, 147 - 157.

Grady(a), D. E., and Kipp, M. E. (1985). Geometric Statistics and Dynamic Fragmentation. *Journal of Applied Physics*, 1210-1222.

Grady(b), D. E., and Kipp, M. E. (1985). Mechanisms of Dynamic Fragmentation: Factors Governing Fragment Size. *Mechanics of Materials*, 311-320.

Granström, S., A. (1956). Loading Characteristics of Air Blasts From Detonating Charges. *Transactions of the Royal Institute of Technology Stockholm, Sweden*.

Griffith, A., A. (1921). VI The Phenomena of Rupture and Flow in Solids. *Philosophical Transactions of the Royal Society A, 221*(582-593), 163-198.

Hibbeler, R. C. (2014). *Mechanics of Materials: Ninth Edition*. Boston: Prentice Hall.

Johnson, R., Salim, H. A., Hoemann, J. M., Nelson, K. M., Bewick, B. T., and Hammons, M. I. (2009). *Validation and Design of Sheet Retrofits*. Retrieved from Defense Technical Information Center: https://apps.dtic.mil/dtic/tr/fulltext/u2/a541354.pdf

Jones, P. A. (1989). *WAC: An Analysis Program for Dynamic Loadings on MAsonry and Reinforced Concrete Walls.* (Masters of Science). Mississippi State, Mississippi State.

Krauthammer, T., and Altenberg, A. (2000). Negative Phase Blast Effects on Glass Panels. *International Journal of Impact Engineering 24*, 1-17.

Magallanes, J. M., Morrill, K. B., Crawford, J. E., Oesterle, M. G., and Hegemeir, G. A. (2008). *Finite Element Models For The Analysis And Design Of CMU Walls To Blast Load.* Paper presented at the Departpent of Defense Explosives Safty Seminar, Palm Springs.

Moradi, L. (2007). *Resistance of Membrane Retrofit Concrete MAsonry Walls to Lateral Pressure*. Retrieved from Tyndall Air Force Base:

National Concrete Masonry Association. (2003). *Annotated Design and Construction Details for Concrete Masonry*. Herndon VA.: National Concrete Masonry Association.

National Research Council. (1995). *Protecting Buildings From Bomb Damage: Transfer of Blast-Effects Mitigation Technologies from Military to Civilian Applications*. Washington: National Academy Press.

Office of Special Technology TSWG GAA Administration. (2002). *Compile and Enhance Blast Related CMU Wall Test Database*. Retrieved from

Rigby, S. E., Tyas, A., Clarke, S. D., and Fay, S. D. (2014). The Negative Phase of the Blast Load. *International Journal of Protective Structures Vol. 5 Num. 1*, 1-19.

Smalley, L. L., and Woosley, J. K. (1999). Application of Steady State Maximum Entropy Methods to High Kinetic Energy Impacts on Ceramic Targets. *International Journal of Impact Engineering*, 869-882.

Teich, M., and Gebbeken, N. (2010). The Influence of the Underpressure Phase on the Dynamic Response of Structures Subjected to Blast Loads. *Internationl Journal of Protective Structures Vol. 1 Num. 2*, 219-233.

The Masonry Society. (2016). *TMS 402/602-16 Building Code Requirements and Specification for Masonry Structures* Longmount: The Masonry Society.

U.S. Army Core of Engineers Protective Design Center. (2008). *Methodology Manual for the Single-Degree-of-Freedom Blast Effects Design Spreadsheets*. Retrieved from https://www.nwo.usace.army.mil/Portals/23/docs/PDC/PDC_TR-05-01_SBEDS_DistribA.pdf?ver=2018-11-01-090139-067

Wiehle, C. K., and Bockholt, J. L. (1968). *Summary of Existing Structures Evaluation Part I: Walls*. Retrieved from Washington D. C.: https://apps.dtic.mil/dtic/tr/fulltext/u2/687293.pdf

Yong, L. K., Xu. (2007). Prediction of debris launch velocity of vented concrete structures under internal blast. *International Journal of Impact Engineering, 34*, 1753-1767.

Zhang, Y.-Q., Lu, Y., and Hao, H. (2004). Analysis of Fragment Size and Ejection Velocity at High Strain Rate. *International Journal of Mechanical Sciences*, 27-34.

*Attempts were made to locate these sources but they could not be located to confirm the information that they contained. They have been listed here to give appropriate credit. They were originally cited by Granström (1956).